



German International University



Technische Hochschule Ulm

Faculty of Informatics and Computer Science

Further development of an AI-Supported Algorithm to choose a suitable Shaft-Hub-Connection

Bachelor Thesis

Author: Farah Hany
Supervisor: Prof. Dr.-Ing. Michael Lätzer
Submission Date: 21 January, 2026



German International University



Technische Hochschule Ulm

Faculty of Informatics and Computer Science

Further development of an AI-Supported Algorithm to choose a suitable Shaft-Hub-Connection

Bachelor Thesis

Author: Farah Hany
Supervisor: Prof. Dr.-Ing. Michael Lätzer
Submission Date: 21 January, 2026

This is to certify that:

- (i) the thesis comprises only my original work toward the Bachelor Degree,
- (ii) due acknowledgement has been made in the text to all other material used.

Farah Hany

21 January, 2026

Acknowledgments

I would like to express my sincere gratitude to my supervisor, Prof. Dr.-Ing. Michael Lätzer, for his continuous guidance, technical insight, and support throughout the development of this thesis.

I would also like to thank my family and friends for their encouragement, patience, and motivation throughout this journey.

Finally, I gratefully acknowledge the previous thesis project “Development of an AI-supported algorithm for the differentiated selection of shaft-hub connections under specific conditions”, which provided a foundation and motivation for the analytical and data-driven approach developed in this work.

AI Usage Statement

This thesis has been developed with the assistance of artificial intelligence tools, primarily for code development, synthetic dataset analysis, and text editing purposes. AI tools, including large language models, were utilized to support the implementation of machine learning algorithms, data preprocessing pipelines, and the analytical scoring system. The use of AI was particularly valuable in exploring different analytical approaches, debugging code, and generating initial drafts of technical documentation.

All research questions, methodological decisions, experimental design, results, and final interpretations remain my own. The AI tools served as assistants in the technical implementation and writing process, but the core research contributions, analytical framework development, and critical evaluation of results were conducted independently. All code, analyses, and conclusions have been carefully reviewed and validated to ensure accuracy and scientific rigor.

Abstract

Shaft–hub connections are essential components used to transmit torque between mechanical elements. A wide variety of connection types exist, and using traditional methods such as engineering judgment and handbook equations, a suitable option can be selected. This thesis develops a model capable of identifying the most appropriate shaft–hub connection among three common alternatives: interference (press) fits, keyed fits, and splined fits, thereby automating the selection process.

A key motivation for this work arises from a practical gap: no publicly available dataset exists for shaft–hub connection selection, making machine-learning approaches difficult to pursue directly. To address this, the first part of the thesis focuses on constructing a synthetic dataset using analytical equations together with a preference-based scoring mechanism. The scoring system incorporates eight user-defined preference dimensions: assembly/disassembly ease, axial movement suitability, manufacturing cost, bidirectional torque capability, vibration resistance, high-speed suitability, maintenance ease, and durability/fatigue life. A pipeline was developed to assign a shaft–hub connection to individual scenarios until the scoring behaviour and feasibility logic achieved satisfactory performance. Once validated, this pipeline was employed as an automated label generator to produce a large and diverse dataset that reflects realistic engineering designs, with input parameters randomized in accordance with DIN standards.

The second part of the thesis develops a classification model trained on this synthetic dataset. The model learns to predict the most suitable connection type based on geometric parameters, material combinations, surface conditions, torque requirements, and user preferences. By integrating analytical constraints with learned behaviour, the resulting classifier captures both practical feasibility relations and subtler preference-driven trade-offs.

To support accessibility and real-world usage, a web-based interface was implemented using FastAPI and React. The interface utilizes the trained machine-learning model for recommendations, presenting the predicted connection type together with its softmax classification score for each query. In addition, analytical torque capacities for all connection types are computed and displayed, providing users with a transparent and interpretable comparison between ML confidence and practical feasibility. Users can freely specify their design parameters and preference values, making the system flexible for educational and practical applications.

The resulting system offers an explainable, data-driven, and mechanically consistent platform. It demonstrates how analytical engineering knowledge can be transformed into

a synthetic dataset for training intelligent models, ultimately improving the accessibility of shaft–hub design expertise and helping users better understand the trade-offs between different connection types.

Contents

Acknowledgments	V
AI Usage Statement	VII
Abstract	IX
1 Introduction	1
1.1 Problem Statement	1
1.2 Task Description	2
1.3 Research Objectives	3
1.4 Contributions	3
1.5 Structure of the Thesis	4
2 Background	5
2.1 Motivation: The Shaft–Hub Connection Selection Problem	5
2.2 Shaft–Hub Connections in Rotating Machinery	6
2.2.1 Friction Closure: Interference (Press) Fits	6
2.2.2 Biaxial Stress State in Press Fits	9
2.2.3 The von Mises Yield Criterion	10
2.2.4 Form Closure: Keys and Splines	12
2.2.5 Comparison of Connection Types	17
2.3 Relevant Industry Standards	17
2.4 Materials and Contact Mechanics	20
2.5 Feasibility Considerations	22
2.6 Preference-Based Engineering Trade-Offs	22
2.7 Synthetic Data in Engineering Design	23
2.8 Machine Learning Concepts for Hybrid Prediction	23
2.8.1 What is Machine Learning?	23
2.8.2 Supervised Classification	24
2.8.3 Tree-Based Models and Gradient Boosting	24
2.8.4 Ensemble Learning	25
2.8.5 Evaluation Metrics and Model Selection	26
2.9 State of the Art in Engineering Design Automation	27
2.10 Summary	30

3 Methodology	35
3.1 Material Database and Engineering Constants	36
3.2 Analytical Selector: Capacity Computations	36
3.2.1 Input Validation	37
3.2.2 Press-Fit Capacity (Friction Closure)	37
3.2.3 Key Capacity (Form Closure)	38
3.2.4 Spline Capacity (Form Closure)	39
3.3 Feasibility Filtering and Preference-Based Scoring	39
3.3.1 Design Torque and Feasibility	40
3.3.2 Connection Performance Profiles	40
3.3.3 Scoring Function	41
3.4 Synthetic Dataset Generation	43
3.4.1 Geometry and Condition Sampling	43
3.4.2 Torque and Safety Factor Sampling	43
3.4.3 Preference Weight Sampling	45
3.4.4 Label Generation	45
3.5 Machine Learning Training and Model Selection	45
3.5.1 Feature Engineering	45
3.5.2 Model Selection Rationale	46
3.5.3 Model Candidates	46
3.5.4 Evaluation Strategy and Metric Selection	46
3.5.5 Model Persistence	47
3.6 Deployment: Backend Service and Web Frontend	47
3.6.1 Backend Architecture	47
3.6.2 Frontend Interface	48
3.6.3 Deployment and Availability	48
3.7 Summary	48
4 Results	51
4.1 Analytical Model Verification	51
4.2 Synthetic Dataset Characteristics	56
4.3 Requirements Validation	59
4.3.1 Requirement R1: Scoring System Accuracy	59
4.3.2 Requirement R2: Dataset Diversity and Coverage	60
4.3.3 Requirement R3: ML Model Performance	60
4.3.4 Requirement R4: System Integration and Usability	60
4.4 Machine Learning Model Performance	61
4.4.1 Error Analysis and Failure Modes	63
4.5 Web Application Demonstration	67
5 Discussion	71
5.1 Analytical Model Behavior and Validity	71
5.2 Effect of Preference-Weighted Scoring	72
5.3 Synthetic Data and ML Model Integration	72

5.4	System-Level Considerations and Limitations	73
6	Conclusion	75
6.1	Research Objectives Revisited	75
6.2	Summary	76
6.3	Relation to Existing Work	76
6.4	Limitations and Future Work	76
6.5	Outlook	77
6.5.1	Integration of Literature and Research Data	77
6.5.2	Enhanced Precision Through Multi-Source Learning	77
6.5.3	Continuous Learning and Model Updates	78
6.5.4	Technical Implementation Considerations	78
6.6	Concluding Remarks	78
Appendix		79
A	Nomenclature	79
B	Lists	82
	List of Abbreviations	82
	List of Figures	85
	List of Tables	86
C	Source Code	87
C.1	Analytical Selector: Core Functions	88
C.1.1	Press-Fit Capacity Calculation	88
C.1.2	Key Capacity Calculation	89
C.1.3	Spline Capacity Calculation	90
C.1.4	Preference Scoring Function	91
C.1.5	Main Selection Function	92
C.2	Synthetic Dataset Generation	93
C.3	Machine Learning Training	94
C.4	Web Application Backend	95
C.5	Web Application Frontend	96
References		97

Chapter 1

Introduction

Shaft–hub connections are fundamental components in mechanical engineering. A rotating shaft transmits torque to an attached component through this interface, and the choice of connection type significantly affects the integrity and performance of the entire system.

An overly conservative selection can introduce unnecessary cost, manufacturing complexity, and maintenance burden, while an under-designed connection that does not satisfy the mechanical transmission requirements can compromise the safety of the entire system, potentially resulting in slippage, deformation, or catastrophic failure. Therefore, it is essential to ensure the connection is strong enough to withstand torque requirements while considering economic constraints and cost efficiency.

This gives rise to the topic of optimal shaft–hub connection selection, which is traditionally done using analytical calculations and expert judgement. However, this process can be time-consuming and impractical in startups that may not have access to specialized consultation and expert knowledge.

1.1 Problem Statement

The problem addressed by this thesis can be formally stated as follows: *Given a set of mechanical design parameters (shaft diameter, required torque, material properties, geometric constraints) and user preferences, determine the most suitable shaft–hub connection type among press fits, keyed fits, and splined fits, while ensuring mechanical feasibility and alignment with application-specific priorities.*

This problem is challenging for several reasons. First, no publicly available labeled dataset exists for shaft–hub connection selection, making direct application of machine-learning approaches infeasible. While large datasets derived from experiments, simulations, or historical design databases do exist, they represent proprietary knowledge held by research institutes and companies and are not accessible for this work. Machine learning models typically require large amounts of training data where the correct answers

are known, in this case, examples of design scenarios paired with their optimal connection types. Second, the selection process involves multiple competing criteria beyond pure mechanical capacity, including cost, manufacturability, maintenance requirements, and application-specific preferences. These trade-offs make the problem inherently multi-objective, requiring a framework that can balance competing priorities. Third, traditional analytical methods require expert knowledge and manual iteration, making them impractical for rapid design exploration or for organizations lacking specialized expertise.

Recent research has demonstrated the potential of machine-learning models to support decision-making across engineering tasks [1], [2]. However, the absence of labeled training data represents a fundamental barrier to applying ML directly to this problem. While recent work has explored AI techniques for specific aspects of shaft–hub connections [3], comprehensive selection frameworks that integrate multiple connection types with preference-based evaluation remain unexplored.

1.2 Task Description

This bachelor thesis addresses the following key aspects:

- **Research on the state of the art and research in AI-supported algorithms:** Comprehensive review of current AI and machine learning applications in engineering design, with particular focus on shaft–hub connection selection and hybrid analytical–ML approaches.
- **Presentation of the current standard for interference fit connections, key fit connections and tooth shaft connections:** Detailed examination of DIN standards (DIN 7190 for press fits, DIN 6885 for keys, DIN 5480 for splines) and their application in analytical capacity calculations.
- **Optimization and generalization of the existing AI software for the differentiated selection of the three shaft–hub connections:** Development of an improved framework building upon previous work [4], incorporating preference-weighted scoring, synthetic data generation, and enhanced model selection.
- **Testing of the AI software using practical examples:** Validation of the analytical models against DIN standards and evaluation of machine learning model performance using comprehensive metrics and statistical analysis.
- **Discussion of the results:** Critical analysis of model behavior, preference-weighted scoring effects, system-level considerations, and limitations of the approach.
- **Documentation:** Complete documentation of the methodology, implementation, results, and deployment, including source code availability and user interface design.

The aim of this thesis is to develop an intelligent tool for assigning a shaft–hub connection type to a given set of mechanical and preference-based inputs. This is achieved through a three-step approach:

1. **Analytical Scoring System:** Design a scoring system derived from analytical equations (based on DIN standards) and user preference weighting. This system can evaluate any design scenario and determine the optimal connection type based on mechanical feasibility and user priorities.
2. **Synthetic Dataset Generation:** Scale up the scoring system to automatically generate thousands of training examples. Input parameters (diameters, torques, materials, preferences) are randomly selected within realistic ranges based on DIN standards, and the scoring system determines the correct connection type for each scenario, creating a labeled dataset for machine learning.
3. **Machine Learning Model:** Train a machine-learning classifier on the synthetic dataset. The model learns to predict connection types by recognizing patterns in the training data, enabling rapid predictions on new design scenarios without requiring full analytical calculations.

This produces a unified tool that blends analytical feasibility logic (ensuring mechanical safety), user preferences (reflecting application priorities), and machine learning (providing fast, probabilistic recommendations). The hybrid approach combines the reliability of physics-based calculations with the efficiency of learned pattern recognition.

1.3 Research Objectives

To achieve the aim of this thesis, the following research objectives are defined:

- Develop a scoring system pipeline capable of assigning a shaft–hub connection label based on input parameters and preference-driven criteria.
- Scale this pipeline to generate a large and diverse synthetic dataset using input parameters randomized in accordance with DIN standards.
- Train and evaluate a machine-learning classification model using the synthetic dataset.
- Integrate the trained model into a web-based application to provide automated shaft–hub connection recommendations.
- Present analytical torque capacities and ML confidence scores to improve transparency and interpretability of the selection process.

1.4 Contributions

This thesis makes the following key contributions:

- An analytical scoring system that evaluates shaft–hub connections using torque-based feasibility rules and preference-weighted criteria.

- A large, labeled synthetic dataset for shaft–hub connection selection, generated through a DIN-compliant automated pipeline and including press fits, keyed fits, and splined fits.
- A trained and evaluated machine-learning classifier capable of predicting the most suitable shaft–hub connection type based on the generated dataset.
- A web-based interface, developed using FastAPI and React, that provides real-time connection recommendations to users.
- A hybrid intelligent framework combining analytical mechanics with machine-learning inference, providing torque capacity outputs and softmax-based confidence scores for each prediction.

1.5 Structure of the Thesis

This thesis is organized as follows. Chapter 1 (Introduction) introduces the motivation, problem statement, research gap, aim, objectives, and contributions of the work. Chapter 2 (Background) provides the necessary background on shaft–hub connections, analytical torque transmission models, relevant machine-learning concepts, state of the art in engineering design automation, and a summary of related work. Chapter 3 (Methodology) describes the methodology, including the development of the analytical scoring system, the synthetic dataset generation pipeline, and the training and evaluation of the machine-learning model. Chapter 4 (Results) reports the results, covering analytical model verification, requirements validation, model performance, analysis of the generated dataset, error analysis, statistical significance testing, and interpretation of prediction behaviour. Chapter 5 (Discussion) discusses the findings and their implications, including analytical model behavior, preference-weighted scoring effects, and system-level considerations. Finally, Chapter 6 (Conclusion) concludes the thesis, revisits the research objectives, summarizes the contributions, addresses limitations, and outlines potential directions for future research. The Appendix provides nomenclature, lists of abbreviations, figures, and tables used throughout the thesis.

Chapter 2

Background

This chapter establishes the theoretical and conceptual background needed to understand the methodology and framework developed in this thesis for shaft–hub connection selection. It covers the mechanical principles involved in torque transmission, the types of shaft–hub connections considered in this thesis along with their key properties, and the role of DIN/ISO standards in feasibility assessment [5], [6], [7]. Since this thesis begins with physics-based calculations and integrates machine learning (ML), essential ML concepts, evaluation metrics, and the motivation for synthetic dataset generation are also presented.

2.1 Motivation: The Shaft–Hub Connection Selection Problem

Shaft–hub connections are essential machine elements that form the mechanical interface between a rotating shaft and a hub, allowing torque and rotational motion to be transmitted reliably without relative slip [8]. These connections play a critical role in rotating machinery including electric motors, gearboxes, pumps, and automotive drive-trains. A suitable connection must transmit required torque with adequate safety, avoid excessive stress concentrations, maintain alignment under dynamic loading, and satisfy manufacturing and maintenance constraints.

Selecting the correct connection type is crucial because failure can lead to slippage, fretting, shaft damage, or catastrophic system failure. Despite their widespread use, no publicly available labelled datasets exist for automated shaft–hub connection selection. While large datasets derived from experiments, simulations, or historical design databases do exist, they represent proprietary knowledge held by research institutes and companies and are not accessible for this work. Industrial practice typically relies on engineer experience, handbook charts, and repeated analytical checks, resulting in a manual and time-consuming design process.

The complexity arises because torque capacity depends on interacting geometric, material, and surface parameters; three distinct connection types (press fit, key, spline) have fundamentally different load paths; user/application preferences often override pure mechanical capacity; and standards (DIN 7190, DIN 6885, DIN 5480) define rules but do not guide connection selection. These observations motivate a hybrid analytical–ML approach: analytical models provide physics-consistent feasibility and transparent capacity values, while ML provides rapid probabilistic recommendations learned from analytically labelled synthetic data, and preference weighting enables application-specific trade-offs.

2.2 Shaft–Hub Connections in Rotating Machinery

Connection types fall into two main categories: *friction closure* and *form closure*. Common designs considered in this thesis are:

- **Interference (press) fits** (friction closure),
- **Parallel keys** (form closure),
- **Splines** (form closure).

Each type exhibits characteristic strengths and limitations. In practice, these trade-offs mean that standards-based feasibility alone rarely determines the final design choice; further analysis is typically needed, especially when multiple connection types are feasible.

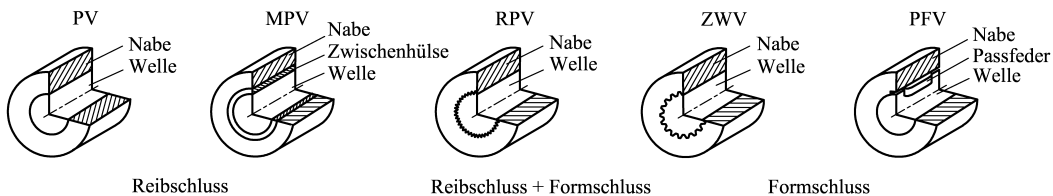


Figure 2.1: Three-dimensional models of different shaft–hub connection types: press fit (PV), multi-part press fit (MPV), knurled press fit (RPV), splined connection (ZWV), and keyed connection (PFV), illustrating the torque transmission mechanisms (friction closure, form closure, or combination) [9].

2.2.1 Friction Closure: Interference (Press) Fits

Press fits transmit torque through friction generated by radial interference between a shaft and a hub [10], [11], [12], [13]. During assembly, the hub may be heated or the shaft cooled (shrink fit), or the parts may be force-assembled at ambient temperature (press fit). After temperature equalisation and elastic recovery, a radial contact pressure p develops at the interface.

For a cylindrical shaft of diameter d and engagement length L , the contact area is

$$A_{\text{contact}} = \pi d L. \quad (2.1)$$

Assuming uniform pressure distribution and a friction coefficient μ , the transmissible torque is

$$M_{t,\text{press}} = \mu p A_{\text{contact}} \frac{d}{2} = \frac{\pi}{2} \mu p L d^2. \quad (2.2)$$

For a required torque M_{req} and a torque safety factor S_R , the required interface pressure, p_{req} , which denotes the minimum interface pressure required for the press-fit connection to safely transmit the factored design torque is

$$p_{\text{req}} = \frac{2M_{\text{req}}S_R}{\pi\mu L d^2}. \quad (2.3)$$

This formulation preserves dimensional consistency and ensures that the safety factor is applied directly to the torque demand, allowing the resulting required pressure to be compared consistently with allowable pressure limits derived from material strength.

Allowable Pressure Considerations The allowable contact pressure p_{allow} represents the maximum interface pressure that can be safely sustained without exceeding material strength limits in either the shaft or hub. This limit is constrained by both components, and the effective allowable pressure is taken as the minimum of the two:

$$p_{\text{allow}} = \min(p_{\text{allow,shaft}}, p_{\text{allow,hub}}). \quad (2.4)$$

To determine these component-specific limits, the allowable stress σ_{zul} for each material is first established based on its strength properties and ductility classification:

$$\sigma_{\text{zul}} = \begin{cases} \sigma_y/S_F, & \text{if ductile,} \\ \sigma_{uts}/S_B, & \text{if brittle,} \end{cases} \quad (2.5)$$

where σ_y is the yield strength, σ_{uts} is the ultimate tensile strength, and S_F and S_B are safety factors for yield-based and ultimate-based limits, respectively.

For ductile materials, the allowable stress is based on the yield strength, since exceeding σ_y initiates plastic deformation that can permanently alter the press-fit geometry and relax the interface pressure, even without fracture. For brittle materials, which exhibit negligible plastic deformation and may fail abruptly by crack initiation and propagation, the ultimate tensile strength σ_{uts} provides a more appropriate basis for limiting failure risk.

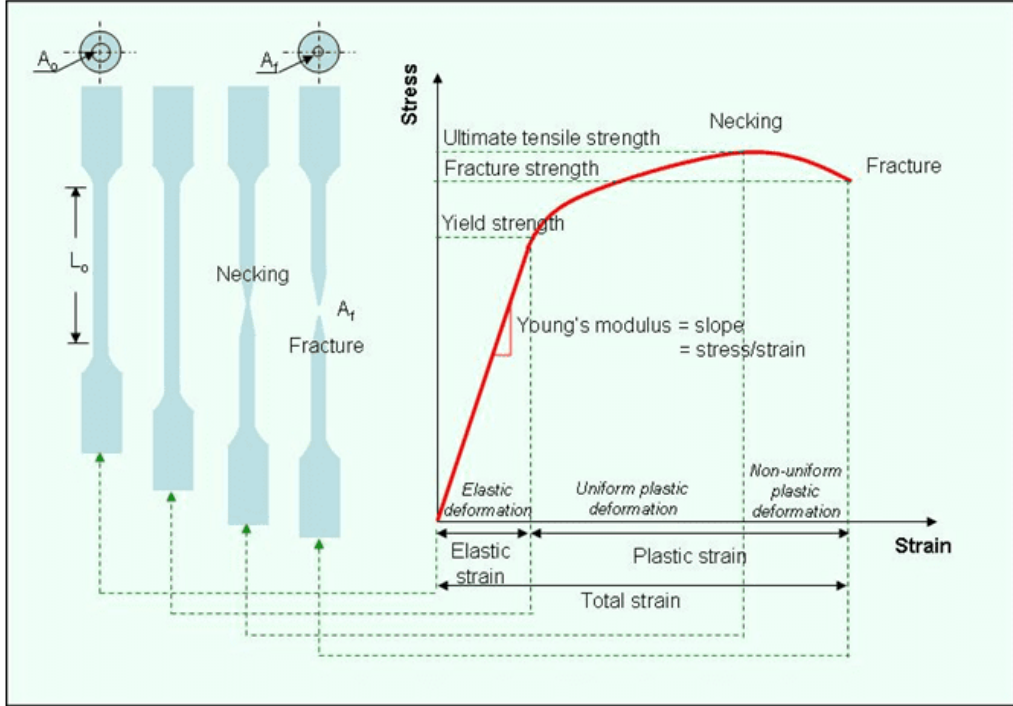


Figure 2.2: Stress–strain curve from a uniaxial tensile test, showing elastic deformation, yield strength, uniform and non-uniform plastic deformation, ultimate tensile strength, and fracture. The curve illustrates the material behavior that forms the basis for von Mises yield criterion, which compares multiaxial stress states to the uniaxial yield strength [14].

The geometric configuration also influences the allowable pressure. For the hub, the diameter ratio

$$Q_A = \frac{d}{D} \quad (2.6)$$

characterizes the hub wall thickness, where D is the hub outer diameter. As $Q_A \rightarrow 1$ (thin-walled hubs), the hub’s ability to sustain interface pressure decreases significantly. For the shaft, the ratio

$$Q_I = \frac{d_i}{d} \quad (2.7)$$

accounts for hollow shafts, where d_i is the inner diameter (zero for solid shafts).

The component-specific pressure limits are then calculated using thick-walled cylinder theory, accounting for the stress state under internal pressure. The hub and shaft pressure limits are:

$$p_{\text{allow,hub}} = \frac{1 - Q_A^2}{\sqrt{3}} \sigma_{\text{zul,hub}}, \quad (2.8)$$

$$p_{\text{allow,shaft}} = \frac{2}{\sqrt{3}} \sigma_{\text{zul,shaft}} (1 - Q_I^2), \quad (2.9)$$

As the diameter ratios $Q_A = d/D$ and $Q_I = d_i/d$ increase, the geometric terms $(1 - Q_A^2)$ and $(1 - Q_I^2)$ decrease, leading to a reduction in the allowable interface pressure. In the hub, increasing Q_A corresponds to a thinner wall, which results in higher circumferential (hoop) stresses and therefore a lower allowable pressure. In the shaft, increasing Q_I reflects increased hollowness, which reduces the load-carrying cross-section and raises the induced stress for a given interface pressure.

The factor $1/\sqrt{3}$ in Equations (2.8) and (2.9) arises from the application of the von Mises equivalent stress criterion to the biaxial stress state in the cylindrical components. To understand this, it is necessary to examine what is meant by a biaxial stress state and why the von Mises criterion is required.

2.2.2 Biaxial Stress State in Press Fits

In a press fit, the shaft and hub are not loaded in just one direction. Because of the interface pressure p , each cylindrical component experiences two principal stresses acting simultaneously and perpendicular to each other creating what is known as a *biaxial stress state*:

- **Radial stress σ_r :** Acts inward (compressive) and is caused directly by the contact pressure at the interface.
- **Circumferential (hoop) stress σ_θ :** Acts around the circumference of the cylinder. In the hub, this stress is tensile, while in the shaft it is compressive. The hoop stress is usually larger in magnitude than the radial stress.

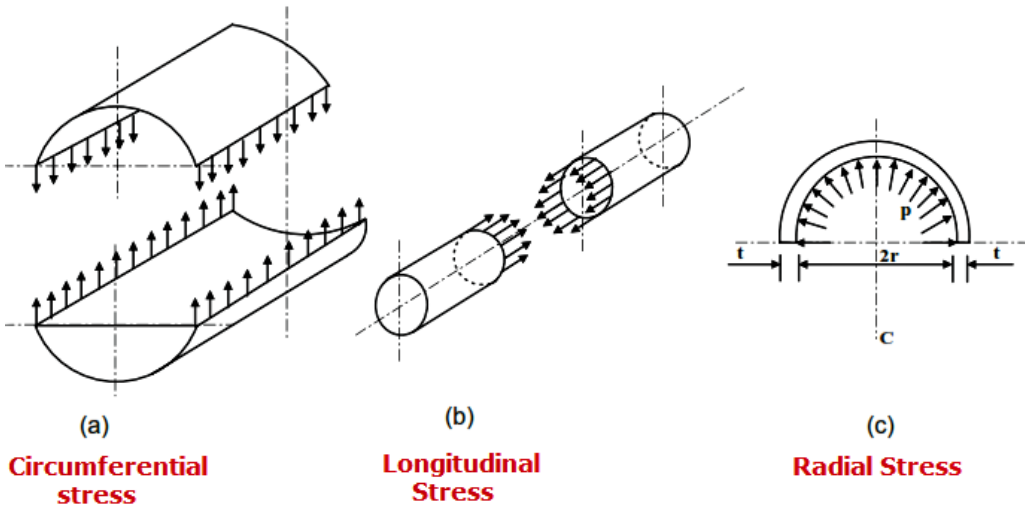


Figure 2.3: Types of stresses in cylindrical components: (a) circumferential (hoop) stress, (b) longitudinal stress, and (c) radial stress. In press fits, the dominant stresses are radial and circumferential, creating a biaxial stress state [15].

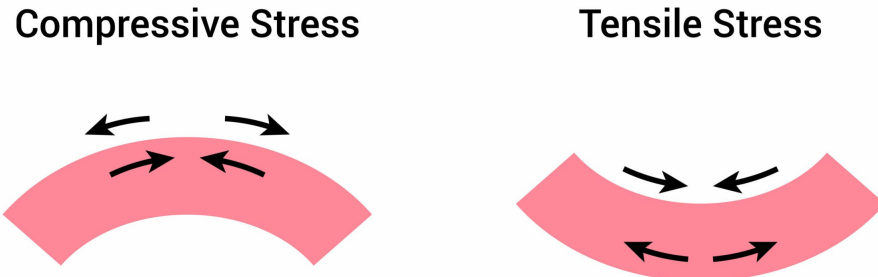


Figure 2.4: Illustration of types of circumferential (hoop) stress in curved components. The direction of arrows indicates how forces cause compression and tension within a material [16].

Materials do not fail because of just radial stress or hoop stress alone; failure occurs because of the combined effect of all stresses acting together. Therefore, a method is needed to combine σ_r and σ_θ into a single equivalent stress value that can be compared to the material's uniaxial yield strength. This is where the von Mises yield criterion provides the solution.

2.2.3 The von Mises Yield Criterion

The von Mises yield criterion states that a ductile material yields when the distortional (shear-related) energy in the material reaches the same level as in a uniaxial tensile test at yield (see Figure 2.2). The key insight is that von Mises converts a multiaxial stress state into an equivalent single stress value, called the von Mises equivalent stress σ_{vM} . This allows safe comparison of σ_{vM} against the allowable stress σ_{zul} .

For a cylinder under internal or external pressure, the axial stress is negligible under the open-ended assumption. The dominant stresses are σ_r and σ_θ , creating a plane (biaxial) stress condition. When these stresses are inserted into the von Mises formula:

$$\sigma_{vM} = \sqrt{\sigma_\theta^2 - \sigma_\theta\sigma_r + \sigma_r^2}, \quad (2.10)$$

and the expressions from thick-walled cylinder theory are substituted, the result simplifies to a form proportional to the interface pressure p . Solving this relation for p introduces the factor $1/\sqrt{3}$.

These different stress distributions lead to different proportionality constants in the pressure limit equations. The additional factor of 2 in the shaft expression (Equation (2.9)) reflects the more favorable compressive stress state of the shaft, allowing

it to tolerate higher interface pressures than the hub. However, both components rely on the same von Mises concept: combining radial and hoop stresses into one equivalent stress that can be compared against the material's yield strength.

Mechanical feasibility requires that the required pressure does not exceed the allowable:

$$p_{\text{req}} \leq p_{\text{allow}}. \quad (2.11)$$

Interference and Torque Capacity The fundamental parameter governing press-fit performance is the *interference*, defined as the amount by which the shaft diameter exceeds the hub bore diameter before assembly. This geometric difference creates the radial contact pressure p at the interface. The relationship between interference and torque capacity follows a direct chain: larger interference leads to higher contact pressure p , which increases the friction force (proportional to μp), and consequently increases the transmissible torque (Equation (2.2)). Therefore, analytically, more interference results in greater torque capacity. However, practical limits exist: extremely high interferences may be torque-feasible in theory but become impractical or damaging during assembly, requiring excessive press forces or thermal methods that can cause material damage or geometric distortion.

Backlash-Free Operation Press fits are inherently backlash-free, meaning they exhibit no play or relative motion under load reversal. Backlash occurs when clearance exists between mating parts, allowing torque reversal to cause relative motion before load is re-engaged. In a press fit, the shaft and hub are in continuous interference contact with no clearance in the circumferential direction. The friction force resists motion in both rotation directions equally, eliminating play under load reversal. This absence of clearance prevents rattle, impact loading, and positioning errors, making press fits particularly suitable for applications requiring precise bidirectional torque transmission and smooth operation.

Excellent Concentricity Press fits provide excellent concentricity, meaning the shaft and hub axes align with high geometric accuracy. In press fits, both parts are cylindrical, and the interference causes self-centering during assembly as the parts naturally seek the position of minimum potential energy. Unlike form-closure connections (keys, splines) that rely on discrete contact points, press fits achieve uniform radial contact around the entire circumference. This uniform contact distribution results in high geometric alignment, making press fits especially suitable for high-speed rotation, low vibration applications, and fatigue-sensitive components where misalignment would cause dynamic unbalance or stress concentrations.

Despite these advantages, press fits are sensitive to several practical factors that limit their applicability. Surface condition directly affects the friction coefficient μ , which governs torque capacity according to Equation (2.2). Contamination, oxidation, or improper

surface finish can significantly reduce friction, compromising torque transmission. Lubrication during assembly or operation can similarly reduce friction, potentially causing slip under load. Assembly constraints pose another challenge: achieving the required interference demands either high press forces (which can damage components or require specialized equipment) or thermal methods (heating hub or cooling shaft), both of which introduce complexity and potential failure modes. Thin hubs are particularly critical, as insufficient wall thickness leads to excessive hub compliance. This compliance can cause non-uniform deformation during assembly, resulting in phenomena such as bell-mouthing (where the hub opening flares outward), which reduces effective contact area and compromises torque capacity. These considerations motivate the additional manufacturability and stiffness checks introduced later in the analytical model to filter out mechanically feasible but practically unrealistic designs.

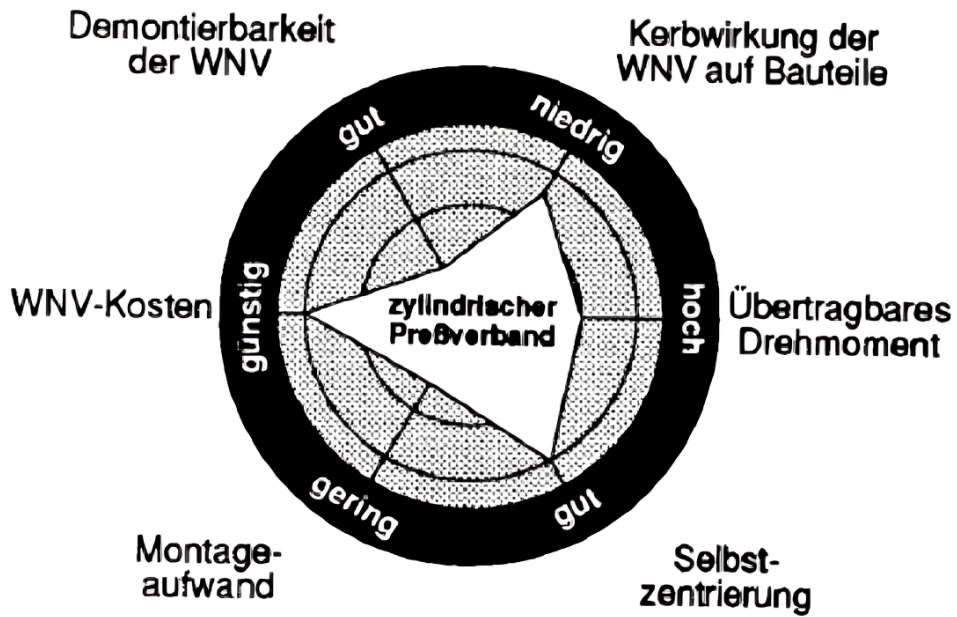


Figure 2.5: Radar chart summarizing qualitative characteristics of a press-fit shaft–hub connection. The chart compares relative strengths and weaknesses across multiple design criteria that are important in practice but difficult to quantify analytically. In the radar chart, values farther from the center indicate better performance, while values closer to the center indicate poorer performance. The filled polygon shows how a cylindrical press fit performs across these criteria. See Table 2.1 for explanation of each axis [13].

2.2.4 Form Closure: Keys and Splines

Form-closure connections transmit torque through geometric interlocking rather than frictional interface pressure. In this work, parallel keys and splines are considered as

representative form-closure solutions.

Keys A rectangular parallel key engages matching keyways in the shaft and hub [10], [12], [13], [17]. Torque transmission is governed by two primary failure modes that must both be considered: shear failure of the key cross-section and bearing (crushing) failure at the contact surfaces between the key and keyway.

Shear failure occurs when the shear stress in the key exceeds the material's allowable shear strength. The key acts as a mechanical fuse, transmitting torque through its cross-sectional area. When the applied torque creates a shear force that exceeds the key's shear capacity, the key fails by shearing across its width. The shear-limited torque capacity is

$$T_\tau = \tau_{\text{allow}} b L \frac{d}{2}, \quad (2.12)$$

where τ_{allow} is the allowable shear stress of the key material, b is the key width, and L is the engagement length.

Bearing failure occurs when the contact pressure between the key flanks and the keyway walls exceeds the allowable bearing pressure of either the key or the keyway material. This failure mode manifests as localized plastic deformation or crushing at the contact surfaces, which can lead to loss of fit and reduced torque capacity. The bearing-pressure-limited capacity is

$$T_p = p_{\text{allow}} \left(\frac{h}{2} \right) L \frac{d}{2}, \quad (2.13)$$

where p_{allow} is the allowable bearing pressure and h is the key height. The factor $h/2$ represents the effective moment arm for the bearing force, corresponding to half the key height where the contact pressure acts.

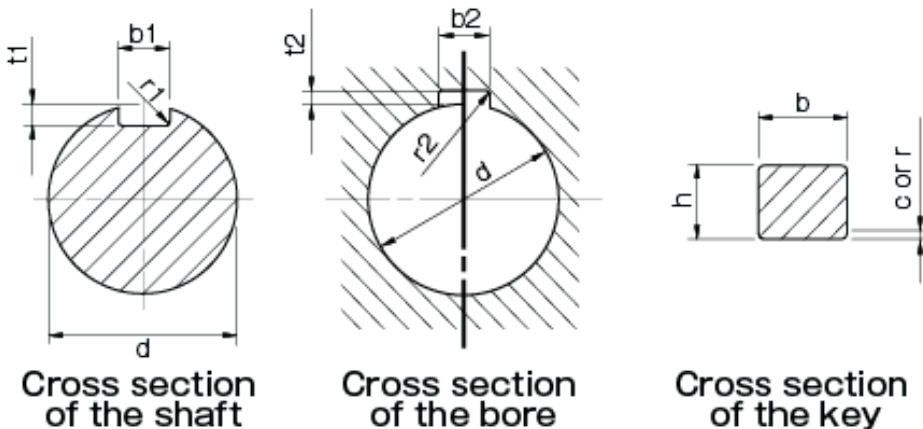


Figure 2.6: Parallel key and keyway fit according to DIN 6885, showing the shaft–hub connection and load-transmitting contact surfaces [18].

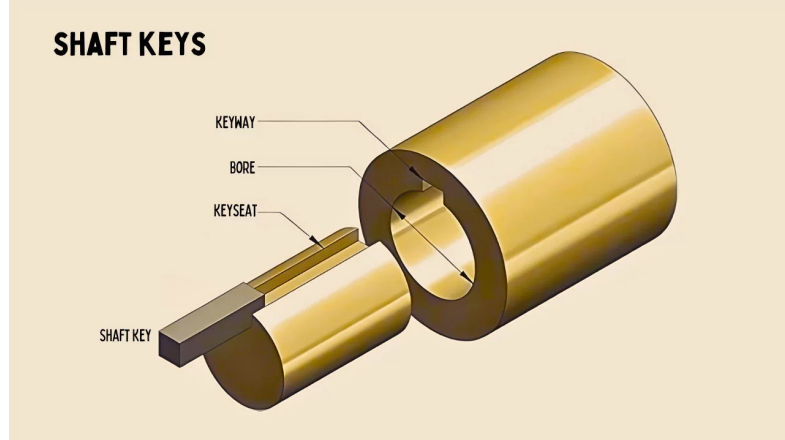


Figure 2.7: Exploded view of a keyed shaft–hub connection, highlighting the key, keyseat (shaft keyway), and hub keyway [19].

The transmissible torque is therefore governed by the more restrictive of these two failure modes:

$$M_{t,\text{key}} = \min (T_\tau, T_p) . \quad (2.14)$$

For keyed connections involving different shaft and hub materials, the allowable bearing pressure p_{allow} used in Equation (2.13) is conservatively taken as the minimum of the shaft and hub material allowables:

$$p_{\text{allow}} = \min (p_{\text{allow,shaft}}, p_{\text{allow,hub}}) . \quad (2.15)$$

This ensures that local contact stresses remain within admissible bounds for both mating parts, with the weaker material governing the design. Keys are inexpensive and easy to assemble and disassemble, but they introduce stress concentrations at the keyway, which can reduce fatigue strength and lead to backlash behavior under reversing loads.

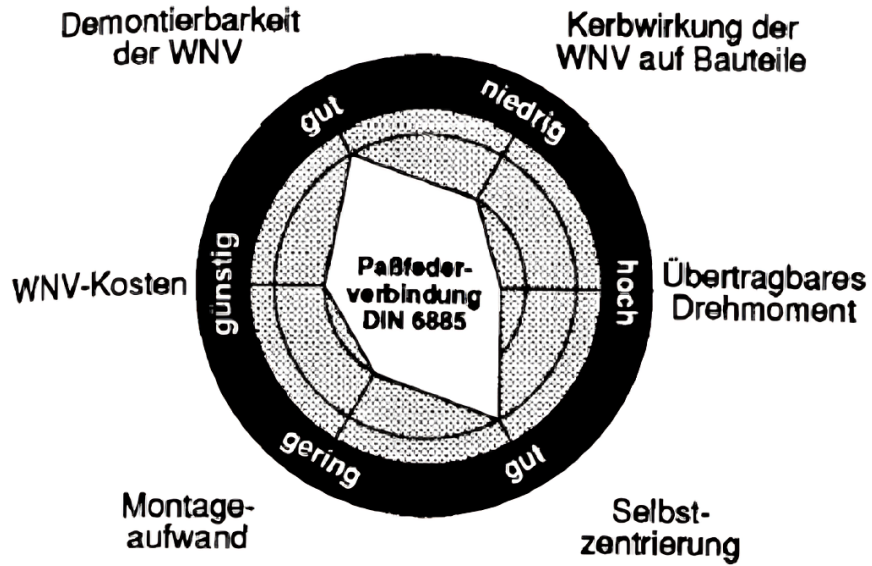


Figure 2.8: Radar chart summarizing qualitative characteristics of a keyed shaft–hub connection (DIN 6885). See Table 2.2 for explanation of each axis [13].

Splines Splines transmit torque through multiple interlocking teeth that engage matching grooves in both the shaft and hub [10], [11], [12], [13]. Unlike keys, which rely on a single rectangular element, splines distribute the load across multiple teeth, significantly increasing load-carrying capacity and improving fatigue performance through load sharing. Each tooth contributes to torque transmission through bearing contact on its flanks (the angled surfaces that engage with the mating spline).

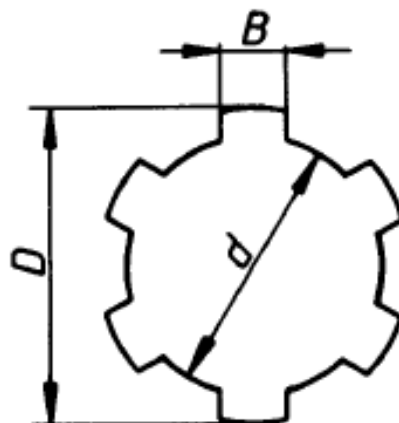


Figure 2.9: Simplified spline cross-section indicating outer diameter D , inner diameter d , and tooth width b used in the analytical formulation [7].

The total projected flank area available for load transmission can be expressed as

$$A_{\text{proj}} = z b h_{\text{proj}}, \quad (2.16)$$

where z is the number of teeth, b is the tooth width (circumferential dimension), and h_{proj} is the projected flank height, given by

$$h_{\text{proj}} = \frac{D - d}{2}, \quad (2.17)$$

where D is the outer diameter and d is the inner diameter of the spline.

In practice, load distribution across spline teeth is not uniform due to manufacturing tolerances, elastic deformation, and geometric misalignment. The teeth closest to the load application point typically carry more load than those farther away. To account for this non-uniform load sharing, the torque capacity calculation uses conservative reduction factors. Rather than using the full projected geometry directly, the torque capacity is based on an effective flank height and a mean radius:

$$M_{t,\text{spline}} = K L z h_{\text{eff}} r_m p_{\text{allow}}, \quad (2.18)$$

where L is the engagement length, r_m is the effective “lever arm” radius at which the tooth contact forces act, and p_{allow} is the maximum allowable contact (bearing) pressure on the spline flanks before local yielding/crushing occurs. The factor K is a conservative load-sharing factor that reduces the ideal capacity to account for the fact that, in reality, not all teeth carry equal load; some teeth are loaded more heavily due to small geometric errors and elastic deformation. In this work, $K = 0.75$ is used to represent these load-sharing losses and practical non-uniformities.

The mean radius r_m represents the effective moment arm for torque transmission:

$$r_m = \frac{d + D}{4}, \quad (2.19)$$

which is the average of the inner and outer radii (a simple way to approximate where the resultant tooth force acts).

The effective flank height h_{eff} accounts for the fact that not all of the projected flank height contributes equally to load transmission. In practice, contact may be non-uniform along the tooth height (e.g., edge contact, micro-misalignment, and manufacturing tolerances), so the full geometric height h_{proj} would overestimate the true load-carrying area. A common conservative approximation is:

$$h_{\text{eff}} \approx 0.8 h_{\text{proj}}. \quad (2.20)$$

This 0.8 factor is therefore an empirical/conservative reduction (not a fundamental geometry identity) used to reflect practical contact conditions and ensure the resulting torque capacity estimate remains realistic.

Splines provide high torque capacity, excellent fatigue behavior, and may be designed for controlled axial sliding. Their main drawbacks are increased manufacturing complexity, tighter tolerances, and higher cost compared to keys and press fits.

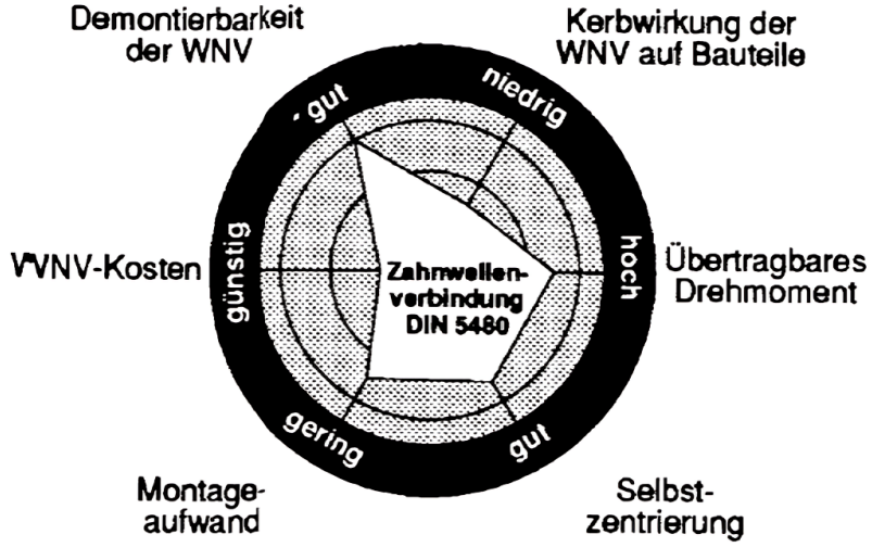


Figure 2.10: Radar chart providing a qualitative assessment of a splined shaft–hub connection according to DIN 5480. See Table 2.3 for explanation of each axis [13].

2.2.5 Comparison of Connection Types

Table 2.4 provides a systematic comparison of the three connection types across key engineering criteria, summarizing their characteristic strengths and limitations.

The comparison reveals that each connection type occupies a distinct niche in the design space. Press fits excel in applications requiring high concentricity, vibration resistance, and zero backlash, but are limited by assembly constraints and inability to accommodate axial movement. Keys offer the best cost–performance trade-off for moderate torque applications with frequent disassembly needs, but suffer from stress concentrations and potential backlash. Splines provide the highest capacity and durability for demanding applications, particularly those requiring axial movement or bidirectional torque, but at significantly higher manufacturing cost.

2.3 Relevant Industry Standards

Several industry standards inform the analytical foundations of the shaft–hub connection models used in this thesis. These standards provide established formulas, geometric

conventions, and limiting criteria for individual connection types. Where standards do not fully specify selection or practical feasibility, conservative engineering heuristics are applied.

- **DIN 7190 (press fits / interference fits)** [5]. This standard forms the basis for modeling friction-closure shaft–hub connections. DIN-style friction coefficients (Haftbeiwerte) for common material pairings and surface conditions are used to estimate torque transmission capability [20]. Figure 2.11 shows the friction coefficient ranges specified in DIN 7190 for different material pairings and surface conditions.

Tabelle 4 — Haftbeiwerte bei Querpressverbänden in Längs- und Umfangsrichtung beim Rutschen

Werkstoffpaarung, Schmierung, Fügung	Haftbeiwerte $\nu_r, \nu_{rl}, \nu_{ru}$
Stahl-Stahl-Paarung	
Druckölverbände normal gefügt mit Mineralöl	0,12
Druckölverbände mit entfetteten Pressflächen mit Glyzerin gefügt	0,18
Schrumpfverband normal nach Erwärmung des Außenteils bis zu 300 °C im Elektroofen	0,14
Schrumpfverband mit entfetteten Pressflächen nach Erwärmung im Elektroofen bis zu 300 °C	0,20
Stahl-Gusseisen-Paarung	
Druckölverbände normal gefügt mit Mineralöl	0,10
Druckölverbände mit entfetteten Pressflächen	0,16
Stahl-MgAl-Paarung, trocken	0,10 bis 0,15
Stahl-CuZn-Paarung, trocken	0,17 bis 0,25

Figure 2.11: Friction coefficients (Haftbeiwerte) for press-fit connections according to DIN 7190, showing ranges for different material pairings and surface conditions [5].

- **DIN 6885 (parallel keys)** [6]. Keyed joints are modeled using standardized key dimensions selected as a function of shaft diameter, consistent with DIN practice. Figure 2.12 illustrates the key dimensions and tolerances specified in DIN 6885. Torque capacity is evaluated based on shear and bearing pressure limits, with conservative allowable values derived from the shaft–hub material combination. The governing capacity is taken as the smaller of these two limits.

Paßfederabmessungen								
Wellendurchmesser d		Breite \times Höhe	Hohe Form (nach DIN 6885 T1)			Hohe Form für Werkzeugmaschinen (nach DIN 6885 T2)		
über	bis	$b \times h$	t_1	t_2	l	t_1	t_2	l
6	8	2 × 2	1,2	1,0	6 ... 20			
8	10	3 × 3	1,8	1,4	6 ... 36			
10	12	4 × 4	2,5	1,8	8 ... 45	3,0	1,1	10 ... 45
12	17	5 × 5	3,0	2,3	10 ... 56	3,8	1,3	12 ... 56
17	22	6 × 6	3,5	2,8	14 ... 70	4,4	1,7	16 ... 70
22	30	8 × 7	4,0	3,3	18 ... 90	5,4	1,7	20 ... 90
30	38	10 × 8	5,0	3,3	22 ... 110	6,0	2,1	25 ... 110
38	44	12 × 8	5,0	3,3	28 ... 140	6,0	2,1	32 ... 140
44	50	14 × 9	5,5	3,8	36 ... 160	6,5	2,6	40 ... 160
50	58	16 × 10	6,0	4,3	45 ... 180	7,5	2,6	45 ... 180
58	65	18 × 11	7,0	4,4	50 ... 200	8,0	3,1	50 ... 200
65	75	20 × 12	7,5	4,9	56 ... 220	8,0	4,1	56 ... 220
75	85	22 × 14	9,0	5,4	63 ... 250	10,0	4,1	63 ... 250
85	95	25 × 14	9,0	5,4	70 ... 280	10,0	4,1	70 ... 250
95	110	28 × 16	10,0	6,4	80 ... 320	11,0	5,1	80 ... 250
110	130	32 × 18	11,0	7,4	90 ... 360	13,0	5,2	90 ... 250
130	150	36 × 20	12,0	8,4	100 ... 400	13,7	6,5	100 ... 250
150	170	40 × 22	13,0	9,4	110 ... 400	14,0	8,2	110 ... 250
170	200	45 × 25	15,0	10,4	125 ... 400			
200	230	50 × 28	17,0	11,4	140 ... 400			

Paßfederlängen l :

6; 8; 10; 12; 14; 16; 18; 20; 22; 25; 28; 32; 36; 40; 45; 50; 56; 63;
70; 80; 90; 100; 110; 125; 140; 160; 180; 200; 220; 250; 280; 320;
360; 400

Figure 2.12: Key dimensions and tolerances for parallel keys according to DIN 6885, showing standardized key sizes as a function of shaft diameter [6].

- **DIN 5480 (splines) [7]**. Splined connections follow a DIN 5480-inspired approach. Figure 2.13 shows the spline geometry and dimensions specified in DIN 5480. For smaller diameters, typical spline geometries are selected from a lookup aligned with standard practice. For larger diameters, a module-based heuristic is used to generate plausible spline geometry parameters. Load sharing is represented through conservative reduction factors applied to the effective flank height and torque capacity.

Tabelle 1. Nennmaße

d mm	Leichte Reihe			Mittlere Reihe				
	Kurzzeichen	N	D mm	B mm	Kurzzeichen	N	D mm	B mm
11					6 x 11 x 14	6	14	3
13					6 x 13 x 16	6	16	3,5
16					6 x 16 x 20	6	20	4
18					6 x 18 x 22	6	22	5
21					6 x 21 x 25	6	25	5
23	6 x 23 x 26	6	26	6	6 x 23 x 28	6	28	6
26	6 x 26 x 30	6	30	6	6 x 26 x 32	6	32	6
28	6 x 28 x 32	6	32	7	6 x 28 x 34	6	34	7
32	6 x 32 x 36	8	36	6	8 x 32 x 38	8	38	6
36	8 x 36 x 40	8	40	7	8 x 36 x 42	8	42	7
42	6 x 42 x 46	8	46	8	8 x 42 x 48	8	48	8
46	6 x 46 x 50	8	50	9	8 x 46 x 54	8	54	9
52	8 x 52 x 58	8	58	10	8 x 52 x 60	8	60	10
56	8 x 56 x 62	8	62	10	8 x 56 x 66	8	65	10
62	8 x 62 x 68	8	68	12	8 x 62 x 72	8	72	12
72	10 x 72 x 78	10	78	12	10 x 72 x 82	10	82	12
82	10 x 82 x 88	10	88	12	10 x 82 x 92	10	92	12
92	10 x 92 x 98	10	96	14	10 x 92 x 102	10	102	14
102	10 x 102 x 108	10	108	16	10 x 102 x 112	10	112	16
112	10 x 112 x 120	10	120	18	10 x 112 x 125	10	125	18

Figure 2.13: Spline geometry and dimensions for involute splines based on reference diameters according to DIN 5480 [7].

In addition to these standards, engineering practicality adjustments are employed to maintain robust and realistic feasibility assessment. While DIN standards define feasibility boundaries, they do not prescribe how to select between multiple feasible connection types. Consequently, this thesis extends standards-based analysis with a preference-weighted and machine-learning-assisted decision framework to support transparent and application-dependent connection selection.

2.4 Materials and Contact Mechanics

Material properties govern allowable stresses, elastic deformation, and compatibility in shaft–hub connections. The materials considered in this work include representative structural and alloy steels (e.g., C45, 42CrMo4), stainless steels, cast irons, bronzes, and aluminum alloys. For each material, a set of mechanical properties is defined, including Young’s modulus E , Poisson’s ratio ν , yield and ultimate tensile strength proxies, and ductility classification. These properties are used to derive safety-factored allowable stresses that limit torque transmission capacity.

The relationship between stress and strain in elastic materials is governed by Hooke's law, which relates normal stress σ to normal strain ϵ through Young's modulus $E = \sigma/\epsilon$, and shear stress τ to shear strain γ through the shear modulus $G = E/[2(1+\nu)]$. Young's modulus E describes how stiff a material is in tension or compression: for a given stress, a higher E means a smaller elastic strain and thus less elastic stretching or squeezing of the component. Poisson's ratio ν characterizes how much a material contracts laterally when stretched (or expands laterally when compressed), and in the linear elastic range is defined as

$$\nu = -\frac{\epsilon_{\text{transverse}}}{\epsilon_{\text{axial}}}. \quad (2.21)$$

Together, E and ν determine how a material deforms elastically under multiaxial loading and enter the press-fit and spline formulations through G and interference-related deformation estimates.

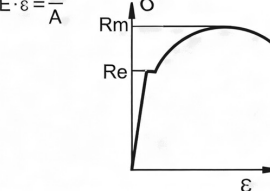
Hooke'sches Gesetz		Werkstoff	Elastizitätsmodul E in N/mm ²	Gleitmodul G in N/mm ²	Querkontraktionszahl ν
Dehnung:	Drillung:				
$\epsilon = \frac{\Delta l}{l_0} = \frac{l - l_0}{l_0}$	$\varphi_t = \frac{\varphi_t}{l}$	Stahl ¹⁾	≈210 000	≈81 000	0,3
$\Delta l = \frac{F \cdot l}{A \cdot E}$	Schlebung: $\gamma = \frac{\varphi_t \cdot r}{l}$	GG	≈100 000	≈38 000	0,25
$\sigma = E \cdot \epsilon = \frac{F}{A}$	Verdrehwinkel: $\varphi_t = \frac{M_t \cdot l}{l_t \cdot G}$	Al-Leg.	≈70 000	≈28 000	0,33
	$\tau = G \cdot \gamma; \tau_{\max} = \frac{M_t}{W_t}$	Gummi	<10	<20	0,49
1) für Federstahl s. II 3/6					

Figure 2.14: Hooke's law relationships for material properties, showing the relationship between stress and strain for normal and shear loading, and the connection between Young's modulus E , shear modulus G , and Poisson's ratio ν [21].

For form-closure connections, allowable shear stresses and permissible bearing pressures are assigned on a material-specific basis. In keyed and splined joints, bearing pressure limits are conservatively governed by the weaker component of the shaft–hub material pair, ensuring that local contact stresses remain within admissible bounds for both mating parts.

For friction-closure connections, contact mechanics are governed by interface pressure and friction. The friction coefficient μ is sensitive to several factors, including:

- material pairing (e.g., steel–steel versus steel–aluminum),
- surface condition (dry or oiled),

- surface roughness.

Conservative friction coefficient ranges inspired by DIN practice are used to estimate torque transmission capacity while maintaining safety against slip. Rather than assigning a single fixed value, friction coefficients are sampled within bounded intervals corresponding to the selected material pairing and surface condition. This approach preserves physical interpretability while introducing controlled variability during synthetic dataset generation.

In addition, elastic material properties, specifically Young's modulus and Poisson's ratio, are used to estimate interference-related deformation effects in press-fit connections. These estimates are employed as plausibility checks that account for elastic recovery and surface roughness losses, allowing mechanically feasible but practically unrealistic designs to be filtered out. Together, these material and contact mechanics considerations provide a physically consistent basis for analytical feasibility assessment and the subsequent decision-making framework developed in this thesis.

2.5 Feasibility Considerations

Before different shaft–hub connection types can be meaningfully compared, basic mechanical feasibility must be ensured. In general, feasibility is established by verifying that a connection can transmit the required torque with an appropriate safety margin, while remaining within admissible material and geometric limits.

Beyond strength-related limits, practical and geometric considerations are commonly required to avoid non-physical or unrealistically difficult designs (e.g., invalid diameter relationships or configurations that are impractical to assemble). In this thesis, these feasibility considerations serve as a prerequisite to the subsequent preference-based evaluation and selection, the detailed formulation and implementation of the feasibility checks are presented in Chapter 3.

2.6 Preference-Based Engineering Trade-Offs

Engineering decisions often involve trade-offs beyond torque capacity alone. Accordingly, this work considers multiple qualitative and semi-quantitative preference dimensions, including:

- assembly and disassembly ease,
- suitability for axial movement,
- cost sensitivity,
- bidirectional torque capability,
- vibration resistance,

- high-speed suitability,
- maintenance effort and accessibility,
- durability and fatigue-related considerations.

Different shaft–hub connection types exhibit characteristic strengths and weaknesses across these dimensions. Incorporating user-defined preference weighting enables selection decisions that reflect application-specific priorities rather than relying solely on mechanical capacity. The detailed formulation of the preference-based evaluation is introduced in Chapter 3.

2.7 Synthetic Data in Engineering Design

Because no labelled datasets exist for shaft–hub connection selection, this thesis relies on *synthetically generated data*, artificially created training examples that simulate real engineering scenarios.

The Need for Synthetic Data. Machine learning models require training data: examples where both the input (design parameters) and the correct output (optimal connection type) are known. In many engineering domains, such labeled datasets don't exist because collecting experimental data is expensive, historical design databases are proprietary, and each design scenario is unique. Synthetic data generation solves this problem by using analytical models as a “labeling oracle” to automatically create thousands of realistic design scenarios and determine the correct connection type for each. The analytical models provide correct answers based on engineering knowledge encoded in standards and design rules, rather than requiring expensive experiments or expert annotation. The detailed data generation procedure is presented in Chapter 3.

2.8 Machine Learning Concepts for Hybrid Prediction

2.8.1 What is Machine Learning?

Machine learning enables computers to learn patterns from data without explicit programming. In this thesis, machine learning complements analytical models by learning subtle patterns and trade-offs that are difficult to encode explicitly in rules. While analytical models provide physically grounded calculations, machine learning captures complex interactions between multiple factors (geometry, materials, preferences) that influence connection selection.

2.8.2 Supervised Classification

Machine learning provides a decision layer to the analytical engineering approach.

Training Process. In supervised classification, the model learns from a training dataset where each example consists of input features (geometric parameters, materials, preferences) and a target label (connection type determined by the analytical scoring system). The dataset is divided into training (70–80%), validation (10–15%), and test (10–20%) sets. The validation set is used for hyperparameter tuning, while the test set provides an unbiased performance estimate. To prevent overfitting, techniques such as regularization, early stopping, and cross-validation are employed to ensure the model learns generalizable patterns rather than memorizing training examples.

2.8.3 Tree-Based Models and Gradient Boosting

Tree-based models are well suited to this problem because they can represent nonlinear decision boundaries that commonly arise from mechanical feasibility constraints and can naturally handle a mixture of numerical and categorical inputs.

Decision Trees. A decision tree is a hierarchical model that makes predictions by asking a series of yes/no questions about input features, branching based on feature values until reaching leaf nodes that provide class predictions. Decision trees can naturally handle both numerical and categorical features, making them well-suited for engineering problems with mixed data types. However, individual trees are prone to overfitting and can be sensitive to small changes in the training data.

Random Forest and Bagging. Random Forest [22] addresses the limitations of single decision trees through *bagging* (bootstrap aggregating). The algorithm trains many independent decision trees, each on a random subset of the training data (bootstrapping) (sampled with replacement). Additionally, at each split, only a random subset of features is considered, introducing diversity among trees. During prediction, all trees vote (aggregation), and the majority class is selected. This ensemble approach reduces overfitting and variance: while individual trees may make errors, their collective decision is more robust. Random Forest provides feature importance scores by measuring how much each feature contributes to reducing impurity across all trees, offering interpretability into which design parameters most influence predictions.

Gradient Boosting. Gradient boosting [23] takes a different ensemble approach: instead of training trees independently, it trains them sequentially, with each new tree focusing on correcting the errors of the previous ensemble. The algorithm starts with a simple model (often a single leaf predicting the average), then iteratively adds trees that

predict the residual errors. Each new tree is trained on the gradient of the loss function with respect to the current predictions, effectively learning to correct mistakes. This sequential learning enables gradient boosting to capture complex, nonlinear relationships that would be difficult for a single tree or independently trained ensemble to learn. The final prediction is the sum of all tree predictions, weighted by a learning rate that controls how aggressively each tree contributes.

Gradient-Boosted Tree Frameworks. This thesis considers several modern gradient-boosted tree frameworks, each with specific optimizations:

- **XGBoost** [24]: Extends gradient boosting with regularization terms (L1 and L2 penalties) to prevent overfitting, and uses second-order optimization (considering both first and second derivatives) for faster convergence. XGBoost also includes built-in handling of missing values and parallel tree construction, making it robust and computationally efficient.
- **LightGBM** [25]: Optimizes training speed and memory usage through histogram-based algorithms that discretize continuous features into bins, reducing the number of split candidates to evaluate. LightGBM uses a leaf-wise (best-first) tree growth strategy instead of level-wise growth, often achieving similar accuracy with fewer trees and faster training times.
- **CatBoost** [26]: Specifically designed for robust handling of categorical variables (such as material names) through a novel method that avoids target leakage during encoding. CatBoost uses ordered boosting, where each tree is trained on a different permutation of the data, reducing overfitting tendencies and improving generalization performance.

2.8.4 Ensemble Learning

In addition to individual classifiers, *ensemble learning* can improve robustness and generalization by combining multiple models. The principle is similar to seeking multiple expert opinions before making an important decision, while individual experts might make mistakes, their collective judgment is often more reliable.

Ensemble Learning and Model Outputs. A soft-voting ensemble combines multiple base classifiers by averaging their predicted class probabilities, reducing variance and improving prediction stability. Machine learning models provide probability estimates for each class, indicating confidence levels. High probabilities suggest confident predictions, while evenly distributed probabilities indicate uncertainty. Tree-based models also provide feature importance scores, identifying which design parameters most influence predictions, validating that the model uses both mechanical constraints and user priorities.

2.8.5 Evaluation Metrics and Model Selection

To assess model performance, this thesis uses several evaluation metrics that provide different perspectives on classification quality. Understanding these metrics requires defining the fundamental classification outcomes for each class: *true positives* (TP), where the model correctly predicts the class; *false positives* (FP), where the model incorrectly predicts the class when it should be another; *true negatives* (TN), where the model correctly predicts a different class; and *false negatives* (FN), where the model incorrectly predicts a different class when it should be the target class.

Confusion Matrix. A confusion matrix provides a detailed breakdown of classification performance by showing how many instances of each true class were predicted as each possible class. For a three-class problem (press fit, key, spline), the confusion matrix is a 3×3 table where rows represent true classes and columns represent predicted classes. Diagonal elements show correct predictions (TP for each class), while off-diagonal elements reveal which classes are confused with which others. The confusion matrix enables qualitative error analysis, identifying systematic misclassification patterns (e.g., whether keys are frequently confused with splines).

Accuracy, Precision, and Recall. *Accuracy* measures the overall percentage of correct predictions:

$$\text{Accuracy} = \frac{\text{TP} + \text{TN}}{\text{TP} + \text{FP} + \text{TN} + \text{FN}} = \frac{\text{Correct Predictions}}{\text{Total Predictions}}. \quad (2.22)$$

While intuitive, accuracy can be misleading with imbalanced classes: a model that always predicts the majority class achieves high accuracy but fails to learn meaningful patterns.

Precision measures the reliability of positive predictions, of all instances predicted as a class, how many were actually that class:

$$\text{Precision} = \frac{\text{TP}}{\text{TP} + \text{FP}}. \quad (2.23)$$

High precision indicates that when the model predicts a class, it is usually correct, reducing false alarms.

Recall (also called sensitivity) measures how well a model finds all instances of a class, of all actual instances of a class, how many were correctly identified:

$$\text{Recall} = \frac{\text{TP}}{\text{TP} + \text{FN}}. \quad (2.24)$$

High recall indicates that the model successfully identifies most instances of a class, reducing missed detections.

F1-Score and Macro-Averaging. Precision and recall often trade off against each other: a conservative model may achieve high precision but low recall (missing many instances), while an aggressive model may achieve high recall but low precision (making many false predictions). The *F1-score* combines precision and recall as their harmonic mean, balancing both concerns:

$$F1 = 2 \cdot \frac{\text{Precision} \cdot \text{Recall}}{\text{Precision} + \text{Recall}} = \frac{2 \cdot TP}{2 \cdot TP + FP + FN}. \quad (2.25)$$

The harmonic mean penalizes extreme imbalances: if either precision or recall is low, the F1-score will be low, encouraging balanced performance.

For multi-class problems, *macro-averaging* computes precision, recall, and F1-score separately for each class, then takes the simple average across all classes:

$$\text{Macro F1} = \frac{1}{C} \sum_{i=1}^C F1_i, \quad (2.26)$$

where C is the number of classes and $F1_i$ is the F1-score for class i . This ensures all classes are weighted equally, preventing dominant classes from masking poor performance on minority classes. In this thesis, model selection is based primarily on macro-averaged F1-score to avoid favoring dominant classes, with the confusion matrix used for qualitative error analysis to understand specific misclassification patterns.

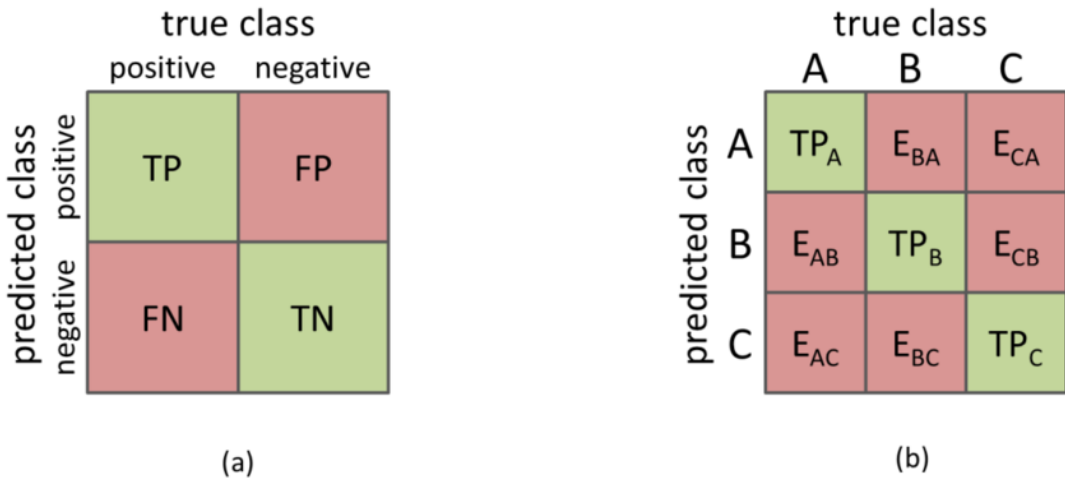


Figure 2.15: Confusion matrix for the three-class problem, showing how predictions are distributed across true and predicted classes [27].

2.9 State of the Art in Engineering Design Automation

The field of engineering design automation has evolved significantly over recent decades, with approaches ranging from purely analytical rule-based systems to data-driven machine-

learning methods [1], [2]. The broader context of Industry 4.0 (Understanding the current landscape helps contextualize the contribution of this thesis) and digitization has accelerated the adoption of AI in engineering processes, creating opportunities for improved efficiency and automation [28], [29]. Understanding the current landscape helps contextualize the contribution of this thesis.

Traditional engineering design relies heavily on analytical calculations derived from first principles and standardized design codes. These methods provide transparent, physically grounded solutions but require expert knowledge and manual iteration. For shaft–hub connections specifically, engineers typically consult handbook charts, perform iterative calculations using DIN standards, and rely on experience to select among feasible options. While reliable, this process is time-consuming and does not scale well to rapid design exploration or automated optimization workflows. Recent work has explored AI techniques for specific aspects of shaft–hub connections, such as improving shrink-fit couplings through machine learning [3], demonstrating the potential for AI-assisted design in this domain. A previous bachelor thesis by Massoud [4] developed an AI-supported algorithm for the differentiated selection of shaft–hub connections using XGBoost and Random Forest, providing a foundation and motivation for the analytical and data-driven approach developed in this work.

Rule-based expert systems emerged as an early attempt to automate engineering decisions. These systems encode expert knowledge as explicit if-then rules, enabling consistent application of design logic. However, they suffer from brittleness; they cannot handle cases outside their predefined rules and require extensive maintenance as knowledge evolves. Moreover, they struggle with multi-criteria trade-offs where multiple factors interact in complex ways.

The advent of machine learning promised to overcome these limitations by learning patterns directly from data. Supervised learning approaches can capture complex, non-linear relationships between design parameters and optimal solutions. However, machine learning requires large, labeled datasets. While such datasets derived from experiments, simulations, or historical design databases do exist, they represent proprietary knowledge held by research institutes and companies and are not publicly accessible. Collecting experimental data is expensive and time-consuming, while extracting historical design data from industry databases faces challenges of data quality, consistency, and proprietary restrictions. At the moment, this work does not have access to these proprietary datasets.

Hybrid approaches that combine analytical models with machine learning have gained traction as a way to leverage the strengths of both paradigms [30], [31], [32]. Physics-informed machine learning incorporates domain knowledge directly into model architectures, ensuring predictions respect physical constraints [30]. Surrogate modeling uses machine learning to approximate expensive simulations, enabling rapid design exploration. However, most hybrid approaches still require some form of training data, whether from simulations or experiments.

Synthetic data generation represents a promising direction for domains lacking empirical datasets. By using analytical models or simulations as labeling oracles, large

datasets can be generated that reflect engineering knowledge encoded in standards and design rules. This approach bridges the gap between rule-based systems and data-driven methods, enabling machine learning while maintaining physical consistency.

The specific problem of shaft–hub connection selection sits at the intersection of these trends. It requires handling multiple competing criteria, respecting mechanical constraints, and providing interpretable recommendations, all while operating in a data-scarce environment. The approach developed in this thesis addresses these challenges by generating synthetic data from analytical models, training machine-learning classifiers on this data, and integrating both components into a unified decision-support system.

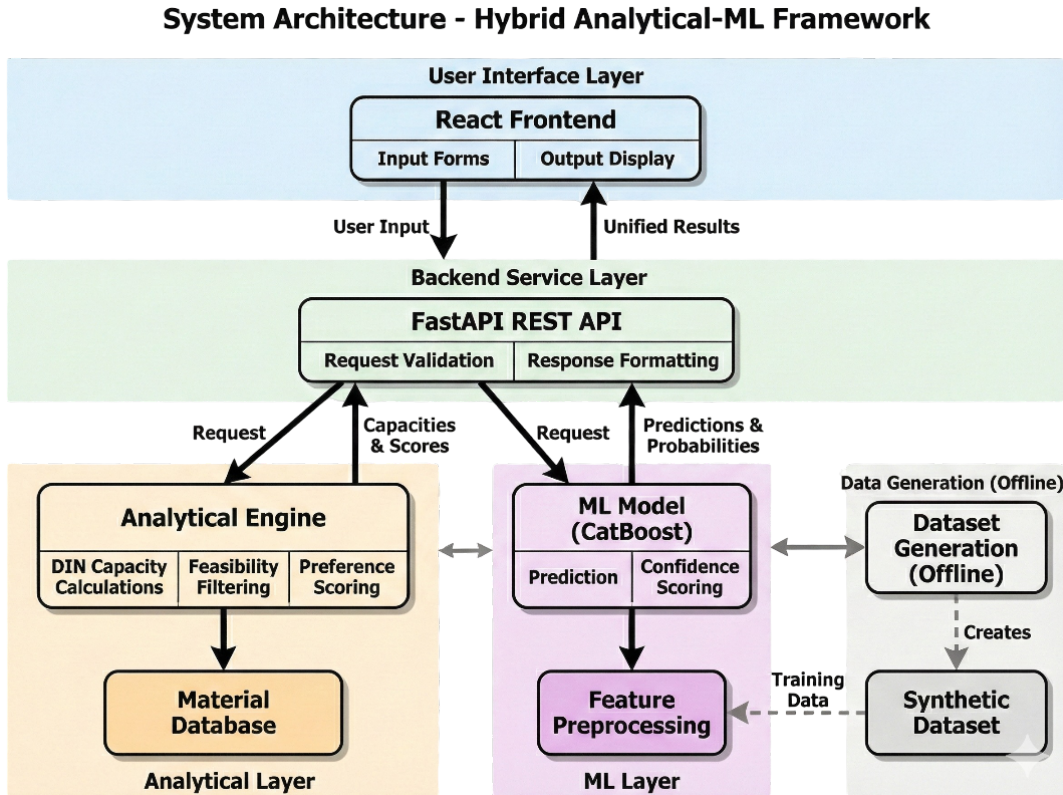


Figure 2.16: System architecture of the proposed hybrid analytical–machine learning framework. User inputs are collected in a React frontend and sent to a FastAPI REST API for request validation and response formatting. The backend executes an analytical engine (DIN-based capacity calculations, feasibility filtering, and preference scoring) supported by a material database, alongside an ML pipeline (feature preprocessing and a CatBoost classifier providing predictions and confidence scores). An offline dataset generation module creates a synthetic dataset used to train the ML component. Source: own illustration.

2.10 Summary

This chapter established the mechanical, analytical, and machine-learning background required to understand the shaft–hub connection selection problem. Fundamental connection types, relevant DIN standards, material and contact mechanics considerations, and preference-based engineering trade-offs were introduced to motivate the need for a structured selection framework. The chapter also outlined the role of synthetic data and supervised machine learning as a means of scaling analytical decision logic in the absence of labelled industrial datasets.

Building on this foundation, the following chapter presents the methodology used to implement a hybrid analytical–machine learning selector, including physics-based feasibility assessment, preference-weighted analytical ranking, synthetic dataset generation, classifier training and evaluation, and system integration.

Table 2.1: Explanation of axes in the press-fit radar chart (Figure 2.5)

Axis	Explanation
Übertragbares Drehmoment (Transmissible torque)	Press fits score high because torque is transmitted over the entire cylindrical surface via friction. This aligns with the analytical model showing strong torque capacity, making press fits excellent for high torque transmission.
Selbstzentrierung (Self-centering)	Rated good. The interference fit naturally aligns shaft and hub concentrically during assembly with no clearance or geometric play, explaining why press fits provide excellent concentricity.
Montageaufwand (Assembly effort)	Rated unfavorable/high effort. Requires high press forces or thermal assembly, controlled tolerances, and specialized equipment, matching the statement about assembly constraints.
WNV-Kosten (Cost of shaft–hub connection)	Rated favorable. No additional components (keys, splines, fasteners) and simple geometry result in low part cost, though tooling and assembly may still be expensive.
Demontierbarkeit der WNV (Disassemblability)	Rated poor. Press fits are often difficult to remove and potentially damaging during disassembly, making them typically permanent or semi-permanent joints.
Kerbwirkung der WNV auf Bauteile (Notch/stress-concentration effect on components)	Rated low. No geometric discontinuities like keyways or spline teeth result in smooth stress distribution, providing a major fatigue advantage of press fits.

Table 2.2: Explanation of axes in the keyed connection radar chart (Figure 2.8)

Axis	Explanation
Übertragbares Drehmoment (Transmissible torque)	Rated moderate to good. Torque is transmitted by form closure via the key. Capacity is limited by key shear and bearing pressure in key and keyway, typically lower than press fits or splines for the same shaft size. Keyed connections provide reliable torque transmission but are not optimal for very high torques.
Selbstzentrierung (Self-centering)	Rated poor. The key does not ensure concentric alignment. Radial positioning relies on shaft–hub clearance and manufacturing accuracy. Keyed joints generally exhibit worse concentricity than press fits or splines.
Montageaufwand (Assembly effort)	Rated low. Simple assembly: insert key and slide hub onto shaft. No high forces or thermal methods required. This is a major practical advantage of keyed connections.
WNV-Kosten (Cost of shaft–hub connection)	Rated favorable. Standardized components (keys per DIN 6885) and simple machining processes make keyed joints cost-effective and widely used.
Demontierbarkeit der WNV (Disassemblability)	Rated good. Hub can be removed easily with no permanent deformation or interference. Well-suited for applications requiring maintenance or frequent disassembly.
Kerbwirkung der WNV auf Bauteile (Notch/stress-concentration effect on components)	Rated unfavorable. Keyways introduce sharp geometric discontinuities and stress concentrations, reducing fatigue strength of shaft and hub. This is the main mechanical disadvantage of keyed connections.

Table 2.3: Explanation of axes in the splined connection radar chart (Figure 2.10)

Axis	Explanation
Übertragbares Drehmoment (Transmissible torque)	Rated high. Torque is transmitted by form closure across multiple spline teeth. Load is distributed over several contact surfaces. Splines provide high torque capacity, especially for larger diameters and higher power levels.
Selbstzentrierung (Self-centering)	Rated good. Involute spline geometry provides accurate radial positioning with improved concentricity compared to keyed connections. Suitable for applications requiring good rotational accuracy.
Montageaufwand (Assembly effort)	Rated moderate. Requires precise manufacturing of spline geometry. Assembly is straightforward once tolerances are met. More complex than keys, but less demanding than press fits.
WNV-Kosten (Cost of shaft–hub connection)	Rated unfavorable to moderate. Higher machining cost due to specialized tooling and tight tolerances. Cost is the main disadvantage of splined connections.
Demontierbarkeit der WNV (Disassemblability)	Rated good. Can be assembled and disassembled repeatedly with no permanent deformation involved. Well-suited for serviceable and modular designs.
Kerbwirkung der WNV auf Bauteile (Notch/stress-concentration effect on components)	Rated moderate. Stress concentrations exist at spline roots, but less severe than keyways due to load sharing and rounded profiles. Better fatigue behavior than keyed connections, but worse than press fits.

Table 2.4: Comparison of shaft–hub connection types

Criterion	Press Fit	Key	Spline
Torque transmission	Friction	Form closure	Form closure
Typical capacity	Moderate	Low–Moderate	High
Assembly/disassembly	Difficult (permanent)	Easy	Moderate
Axial movement	Not possible	Limited	Excellent
Manufacturing cost	Moderate	Low	High
Bidirectional torque	Good	Moderate	Excellent
Vibration resistance	Excellent	Moderate	Good
High-speed suitability	Excellent	Moderate	Good
Maintenance ease	Poor	Good	Moderate
Durability/fatigue	Good	Moderate	Excellent
Concentricity	Excellent	Good	Excellent
Backlash	None	Possible	Minimal
Stress concentration	Low	High (keyway)	Low
Standard	DIN 7190	DIN 6885	DIN 5480

Chapter 3

Methodology

This chapter presents the methodology used to develop the hybrid analytical–machine learning framework for shaft–hub connection selection. The approach addresses the research gap established in Chapter 2: because no publicly available labelled dataset exists for this selection task, the methodology constructs one by first building a physics-based analytical selector, then using it as an automated labeling oracle. A supervised classifier trained on the resulting synthetic data is subsequently integrated alongside the analytical engine into a deployable decision-support tool.

The methodology proceeds through four stages, each building on the previous:

1. **Analytical selector development.** Torque capacities for press fits, keys, and splines are computed using DIN-based equations. Candidates that fail to meet the factored design torque are rejected; press fits undergo an additional manufacturability check to exclude impractical interference values. Feasible candidates are ranked using a preference-weighted scoring function that combines capacity margin and user preferences.
2. **Synthetic dataset generation.** Geometry, torque demand, materials, surface conditions, and preference weights are sampled within realistic, DIN-consistent ranges. Each sample is passed through the analytical selector, and the resulting recommendation becomes the class label. Infeasible samples are discarded to avoid an ambiguous “none” class.
3. **Machine learning training.** Multiple tree-based classifiers are trained on the synthetic dataset. Models are compared using macro F1-score to ensure balanced performance across all connection classes, and the best-performing model is persisted with full preprocessing metadata.
4. **Deployment.** The analytical selector and trained classifier are integrated into a FastAPI backend. A React-based frontend collects user inputs and displays both the analytical recommendation (with capacities, feasibility status, and scores) and the ML prediction (with class probabilities), enabling side-by-side comparison and transparent decision-making.

The remainder of this chapter details each stage: Section 3.1 describes the material database; Sections 3.2 and 3.3 cover the analytical capacity models and scoring logic; Section 3.4 explains the dataset generation process; Section 3.5 presents the ML training pipeline; and Section 3.6 describes the backend and frontend integration.

3.1 Material Database and Engineering Constants

Before capacity calculations can proceed, the system requires access to material properties and application-specific allowables. A curated material database stores the following properties for each entry:

- elastic constants: Young’s modulus E and Poisson’s ratio ν ,
- strength values: yield strength σ_y and ultimate tensile strength σ_{uts} ,
- a ductility flag distinguishing ductile from brittle behavior,
- safety modifiers S_F (for yield-based limits) and S_B (for ultimate-based limits),
- a material category (steel, cast iron, bronze, or aluminum) used for friction coefficient lookup.

The database covers typical engineering materials: structural and alloy steels (S235, C45, 42CrMo4, E360, 16MnCr5), stainless steel (304), cast irons (GG25, GGG40), bronze (CuSn8), and aluminum alloys (6061, 7075). Each material also stores three application allowables:

$$\begin{aligned} \tau_{\text{allow},\text{key}} & \quad (\text{key shear allowable}), \\ p_{\text{allow},\text{key}} & \quad (\text{keyway bearing allowable}), \\ p_{\text{allow},\text{spline}} & \quad (\text{spline flank bearing allowable}). \end{aligned} \tag{3.1}$$

For connections involving two different materials (e.g., a steel shaft in a bronze hub), the effective allowable is taken as the minimum of both components:

$$p_{\text{allow},\text{eff}} = \min(p_{\text{allow},\text{shaft}}, p_{\text{allow},\text{hub}}). \tag{3.2}$$

This conservative rule ensures that neither component exceeds its local stress limits.

3.2 Analytical Selector: Capacity Computations

The analytical selector evaluates three connection types: press fits, keyed joints, and splines, by computing their torque capacities from first principles. Each capacity model draws on the material database and standardized geometry tables to produce physically meaningful results.

3.2.1 Input Validation

Every request undergoes validation before capacity calculations begin:

- **Material availability:** both shaft and hub materials must exist in the database.
- **Shaft type:** restricted to `solid` or `hollow`; hollow shafts require an inner diameter d_i satisfying $0 < d_i < d$.
- **Required torque:** a mandatory positive value M_{req} (in Nmm).
- **Hub geometry:** outer diameter $D > d$ (defaulting to $2d$ if unspecified); engagement length L (defaulting to $1.5d$).

Invalid inputs raise descriptive exceptions, preventing nonsensical configurations from propagating through the system or corrupting the synthetic dataset.

3.2.2 Press-Fit Capacity (Friction Closure)

Press fits transmit torque through friction generated by interface pressure arising from elastic interference. The capacity calculation proceeds in two stages: determining the allowable interface pressure, then computing the resulting torque capacity.

Friction coefficient selection. The friction factor μ (termed *Haftbeiwert* in DIN 7190-1) represents the achievable tangential traction at the interface [5], [20]. The system stores conservative ranges keyed by material-category pairs and surface condition (`dry` or `oiled`). For example, steel–steel dry fits use $\mu \in [0.14, 0.20]$, while steel–cast iron oiled fits use $\mu = 0.10$. Given a request, μ is sampled uniformly from the applicable range:

$$\mu \sim \mathcal{U}(\mu_{\min}, \mu_{\max}), \quad (3.3)$$

introducing controlled variability that later enriches the synthetic dataset. A user override is supported but clamped to $[0.05, 0.25]$ to prevent unrealistic friction assumptions.

Allowable pressure. The permissible interface pressure p_{zul} depends on material strength, ductility, and geometric ratios. Defining

$$Q_A = \frac{d}{D}, \quad Q_I = \frac{d_i}{d} \quad (\text{zero for solid shafts}), \quad (3.4)$$

the allowable stress for each component is:

$$\sigma_{\text{zul}} = \begin{cases} \sigma_y/S_F, & \text{if ductile,} \\ \sigma_{uts}/S_B, & \text{if brittle.} \end{cases} \quad (3.5)$$

The hub and shaft pressure limits are then:

$$p_{\text{hub}} = \frac{1 - Q_A^2}{\sqrt{3}} \sigma_{\text{zul,hub}}, \quad (3.6)$$

$$p_{\text{shaft}} = \frac{2}{\sqrt{3}} \sigma_{\text{zul,shaft}} (1 - Q_I^2), \quad (3.7)$$

with the governing limit $p_{\text{zul}} = \min(p_{\text{hub}}, p_{\text{shaft}})$.

Torque capacity. Using the allowable pressure, the press-fit torque capacity is:

$$M_{t,\text{press}} = \frac{\pi}{2} \mu p_{\text{zul}} L d^2. \quad (3.8)$$

Manufacturability filter. A press fit can be torque-feasible but impractical if it requires excessive interference. The selector therefore evaluates an interference plausibility check. First, the required interface pressure for a given torque with safety factor S_R is:

$$p_{\text{req}} = \frac{2 M_{\text{req}} S_R}{\pi \mu d^2 L}. \quad (3.9)$$

The elastic interference U_e is computed from combined compliance:

$$U_e = p_{\text{req}} d \left[\frac{1 + \nu_I}{E_I(1 - Q_I^2)} + \frac{1 + \nu_A}{E_A(1 - Q_A^2)} \right], \quad (3.10)$$

where subscripts I and A denote shaft and hub respectively. Surface roughness reduces effective interference through a smoothing loss:

$$G = 0.4 \frac{Rz_{\text{shaft}} + Rz_{\text{hub}}}{1000}, \quad (3.11)$$

with roughness values in μm and G in mm. The working interference is $U_w = U_e - G$, subject to the limits:

$$U_w \leq \begin{cases} 0.02 \text{ mm}, & d \leq 50 \text{ mm}, \\ 0.05 \text{ mm}, & d > 50 \text{ mm}. \end{cases} \quad (3.12)$$

If $U_w \leq 0$ (roughness consumes interference) or U_w exceeds the limit, the press-fit candidate is rejected regardless of its torque capacity.

3.2.3 Key Capacity (Form Closure)

Keys transmit torque through shear and bearing at the key–keyway interface. Geometry is determined from a standardized lookup table mapping shaft diameter d to key width b and height h per DIN 6885 [6]. Two failure modes govern capacity:

$$T_\tau = \tau_{\text{allow}} b L \frac{d}{2} \quad (\text{shear}), \quad (3.13)$$

$$T_p = p_{\text{allow,eff}} \frac{h}{2} L \frac{d}{2} \quad (\text{bearing}), \quad (3.14)$$

with the key torque capacity:

$$M_{t,\text{key}} = \min(T_\tau, T_p). \quad (3.15)$$

The shear allowable τ_{allow} comes from the shaft material (the key is typically made from the same or weaker stock), while $p_{\text{allow,eff}}$ uses the weaker of shaft/hub bearing allowables.

3.2.4 Spline Capacity (Form Closure)

Spline geometry is determined from a lookup table for diameters up to 112 mm, providing major diameter D , tooth count z , and width B . Beyond this range, a DIN 5480-like heuristic [7] is used to generate reasonable default geometry. First, a *module* m is chosen from a standard series (e.g. $m = 2, 2.5, 3, \dots$). The module plays the same role as in gear design: it is a length scale that sets the tooth size; choosing from a standard series ensures that the resulting spline is compatible with commercially available tools and profiles. For a given shaft diameter d , the pitch-circle circumference is approximately πd , and the circular pitch is πm , so the number of teeth is roughly

$$z \approx \frac{\pi d}{\pi m} = \frac{d}{m}.$$

This relationship $z \approx d/m$ is therefore a simple geometric consequence of “how many tooth pitches fit around the circumference” for a chosen module. To complete the geometry, the heuristic assigns a projected tooth height h_{proj} proportional to the module, for example

$$h_{\text{proj}} \approx 1.25 m, \quad (3.16)$$

which is consistent with typical DIN 5480 proportions for involute splines. Using the definition $h_{\text{proj}} = 0.5(D - d)$, the major diameter is then computed as

$$D = d + 2 h_{\text{proj}} = d + 2 \cdot 1.25 m. \quad (3.17)$$

This provides a simple, scalable rule for estimating D from d and m when tabulated values are not available. User overrides for D and z are supported and validated when more precise catalogue values are available.

Capacity is computed via an effective flank model:

$$r_m = \frac{d + D}{4}, \quad h_{\text{eff}} = 0.8 h_{\text{proj}}, \quad (3.18)$$

where $h_{\text{proj}} = 0.5(D - d)$. The spline torque capacity is:

$$M_{t,\text{spline}} = K L z h_{\text{eff}} r_m p_{\text{allow,eff}}, \quad (3.19)$$

with $K = 0.75$ representing load-sharing losses and practical non-uniformities.

3.3 Feasibility Filtering and Preference-Based Scoring

With capacities computed for all three connection types, the selector applies a two-stage decision process: first filtering infeasible candidates, then ranking feasible options using a preference-weighted scoring model.

3.3.1 Design Torque and Feasibility

The design torque incorporates the user-specified safety factor:

$$M_{\text{design}} = M_{\text{req}} \cdot S. \quad (3.20)$$

A candidate is feasible if its capacity meets or exceeds the design torque: $M_t \geq M_{\text{design}}$. Press fits additionally require that the interference plausibility check passes. If no candidate is feasible, the selector returns `none` with an explicit reason, for example, “press-fit torque OK but rejected by interference check.”

3.3.2 Connection Performance Profiles

Each connection type is assigned a fixed performance profile across eight application dimensions:

- assembly/disassembly ease,
- axial movement suitability,
- manufacturing cost,
- bidirectional torque capability,
- vibration resistance,
- high-speed suitability,
- maintenance ease,
- durability/fatigue life.

Profile Values. Table 3.1 summarizes the normalized profile values (0.0–1.0) assigned to each connection type for the eight application dimensions.

Table 3.1: Normalized performance profiles for shaft–hub connections across eight application dimensions (0.0 = very poor, 1.0 = excellent). These values are author-defined heuristic estimates based on engineering design guidelines and expert judgment, representing relative performance characteristics of each connection type.

Connection type	Assembly	Axial move.	Cost	Bidirectional	Vibration	High-speed	Maint.	Durability
Press fit	0.20	0.10	0.70	0.80	0.85	0.90	0.25	0.75
Key	0.75	0.30	0.50	0.70	0.45	0.55	0.80	0.40
Spline	0.40	0.95	0.20	0.90	0.70	0.75	0.30	0.85

Profile Assignment Rationale. The profile values encode domain knowledge about how each connection type performs across different application requirements. **Press fits** score very high on vibration resistance and high-speed suitability due to excellent concentricity and the absence of backlash, but very low on assembly/disassembly ease and maintenance because they are essentially permanent connections. **Keys** provide a balanced, low-cost solution with good assembly/disassembly and maintenance behaviour, but lower vibration resistance and durability because keyways introduce backlash and stress concentrations. **Splines** offer excellent axial movement, bidirectional torque transmission, and high durability through load sharing across many teeth, but they are expensive to manufacture and more demanding to maintain. These profiles remain constant across all requests and were calibrated qualitatively using design guides and expert judgment, so that the scoring function can reflect typical engineering trade-offs even when explicit preference weights are moderate.

3.3.3 Scoring Function

The scoring function transforms mechanical capacity and user preferences into a single numerical score that enables ranking of feasible connection candidates [33], [34]. The function is designed to balance multiple competing objectives: mechanical safety margins, economic efficiency, and alignment with user priorities.

Users specify preference weights for each dimension (0.0–1.0 in 0.1 increments), where 0.0 indicates the dimension is unimportant and 1.0 indicates it is critical. The scoring function combines four primary terms:

Margin Reward Term. A connection providing capacity surplus above design torque is preferable, offering a safety buffer. However, the value of additional margin diminishes as capacity increases. The margin reward is:

$$s_{\text{margin}} = w_{\text{margin}} \cdot \min \left(1, \frac{M_t - M_{\text{design}}}{0.35 M_{\text{design}}} \right), \quad (3.21)$$

where M_t is torque capacity and M_{design} is design torque. This term rewards connections with positive margin up to a cap of 35% above design torque. When margin is less than or equal to 35%, the reward scales linearly from 0 (at zero margin) to $w_{\text{margin}} = 0.10$ (at 35% margin). When margin exceeds 35%, the reward saturates at 0.10 and does not increase further. The cap at 35% (0.35) reflects engineering practice for static shaft design: utilization levels of roughly 60–80% of material strength are generally regarded as both safe and economical [10]. A 35% torque margin corresponds to operating in this recommended range while still providing reserve against uncertainties in loads, material scatter, and modelling assumptions.

Overdesign Penalty Term. Excessive overdesign is penalized to avoid selecting unnecessarily large or complex connections when simpler alternatives are adequate. The penalty is:

$$s_{\text{overkill}} = -w_{\text{overkill}} \cdot \min \left(0.5, \frac{M_t - M_{\text{design}}}{M_{\text{design}}} - 0.35 \right)^+, \quad (3.22)$$

where $(\cdot)^+$ denotes the positive part (i.e., $\max(0, \cdot)$). This term works in conjunction with the margin reward: when margin is less than or equal to 35%, the expression $(M_t - M_{\text{design}})/M_{\text{design}} - 0.35$ is negative or zero, so $(\cdot)^+ = 0$ and the penalty is zero. When margin exceeds 35%, the penalty activates and scales with the excess margin above 35%, bounded at 0.5 to prevent extreme penalties. The weight $w_{\text{overkill}} = 0.10$ balances the penalty against other terms. Together, these two terms encode the engineering judgment that margins up to 35% are desirable (rewarded), while margins beyond 35% are treated as over-dimensioned in design guides such as [13], where engineers are encouraged to reduce size or choose a simpler connection instead of keeping excessive reserve.

Preference Utility Term. This term quantifies how well a connection type aligns with user priorities across the eight application dimensions:

$$s_{\text{prefs}} = w_{\text{prefs}} \cdot \frac{\sum_{i=1}^8 u_i \cdot p_i}{\sum_{i=1}^8 u_i}, \quad (3.23)$$

where u_i are user preference weights and p_i are connection profile scores. The denominator normalizes by the sum of user weights, ensuring utility remains bounded between 0.0 and 1.0. If all weights are zero, the denominator defaults to 1.0 and the system falls back to mechanical criteria alone. The weight $w_{\text{prefs}} = 0.70$ is the largest component, reflecting that user preferences are the primary differentiator when multiple connections are mechanically feasible.

Connection-Specific Penalty Terms. Two additional penalty terms address connection-specific practical considerations: (1) **Hub stiffness penalty (press fits):** When $Q_A = d/D > 0.5$, thin-walled hubs are susceptible to deformation during assembly. The penalty is $s_{\text{hub_stiffness}} = w_{\text{hub_stiffness}} \cdot (f_{\text{hub}} - 1.0)$, where f_{hub} decreases from 1.0 to 0.1 as Q_A increases from 0.5 to 0.8, with $w_{\text{hub_stiffness}} = 0.10$. (2) **Spline practicality penalty:** If the user does not value spline advantages (axial movement, bidirectional capability, durability), a simpler connection is more appropriate. The penalty is $s_{\text{spline_practicality}} = -0.2 \cdot \max(0, 1.0 - (u_{\text{movement}} + u_{\text{bidirectional}} + u_{\text{durability}})/3)$, reaching -0.2 when none are valued and zero when all are at maximum.

Composite Score Calculation. The final score for each feasible candidate is the sum of all terms:

$$s_{\text{total}} = s_{\text{margin}} + s_{\text{overkill}} + s_{\text{prefs}} + s_{\text{hub_stiffness}} + s_{\text{spline_practicality}}. \quad (3.24)$$

The feasible candidate with the highest composite score becomes the analytical recommendation. To prevent extreme negative scores from connection-specific penalties from completely eliminating otherwise reasonable candidates, the final score is clamped to a minimum of -0.15. This ensures that even penalized connections remain in consideration if they are the only feasible option or if user preferences strongly favor them despite the penalties.

All intermediate values (capacities, individual score terms, interference diagnostics) are retained in the response for transparency, allowing users to understand why a particular connection was recommended and how close alternative options were to being selected.

3.4 Synthetic Dataset Generation

Because no labeled dataset exists for shaft–hub connection selection, the analytical selector serves as an automated labeling oracle [35], [36]. A synthetic dataset is generated by sampling realistic input configurations and recording the analytical recommendation as the ground-truth label.

3.4.1 Geometry and Condition Sampling

Each sample is drawn from distributions designed to reflect realistic engineering practice:

- **Diameter:** sampled from a discrete DIN-like progression (6–230 mm), with 70% probability mass concentrated in common ranges (20–60 mm), 25% in mid-ranges (60–120 mm), and 5% in tails.
- **Hub length:** proportional to diameter; bending-dominated cases use $L \approx 0.9d - 1.3d$, while non-bending cases use $L \approx 0.4d - 0.8d$.
- **Shaft type:** 80% solid, 20% hollow; hollow shafts sample $d_i \in [0.3d, 0.6d]$.
- **Hub outer diameter:** sampled in $D \in [1.8d, 2.6d]$ with slight increases for bending cases.
- **Surface condition:** dry or oiled with equal probability; 15% of samples include a friction coefficient override.
- **Material:** sampled uniformly from the material database; shaft and hub use the same material to maintain internal coherence.

3.4.2 Torque and Safety Factor Sampling

Torque sampling is designed to generate realistic design scenarios that reflect engineering practice. Rather than sampling torque values directly, the approach uses a diameter-dependent reference torque based on the polar section modulus of the shaft, which scales naturally with shaft size.

Torque Reference Calculation. Torque is sampled relative to a diameter-dependent reference based on the polar section modulus:

$$M_{\text{ref}} = 0.05 \cdot c \cdot \frac{\pi d^3}{16} \cdot f_{\text{taper}}, \quad (3.25)$$

where c is a torque coefficient (typically in the range 1.0–2.0) and f_{taper} is a taper factor that reduces torque demand for larger diameters to reflect practical design trends where larger shafts often operate at lower relative stress levels. The factor f_{taper} takes values of 0.9 for $d > 40$ mm and 0.8 for $d > 70$ mm, with $f_{\text{taper}} = 1.0$ for smaller diameters. The polar section modulus term $\pi d^3/16$ represents the torsional resistance of a solid circular shaft, providing a physically meaningful scaling relationship [10], [11]. The coefficient 0.05 is a scaling factor calibrated to generate reference torques that align with typical engineering practice for shaft–hub connections across the diameter range of interest. A multiplicative factor sampled uniformly from [0.3, 1.4] is then applied to M_{ref} to generate actual torque requirements, creating cases ranging from conservative (30% of reference) to demanding (140% of reference).

Safety Factor Sampling. Safety factors are sampled around a baseline of 1.5, which represents a typical safety margin for static design scenarios in mechanical engineering [10]. The baseline is adjusted based on several factors that influence design conservatism:

- **Bending present:** +0.10 to account for combined loading effects that increase failure risk.
- **Dry surface condition:** +0.05 to reflect reduced friction reliability compared to oiled surfaces.
- **Friction override:** −0.05 when user explicitly specifies friction, indicating confidence in the value.
- **Torque factor exceeding reference:** $+0.20 \cdot (\text{factor} - 1)$ to increase safety margin for demanding torque requirements.
- **Durability preference:** $+0.20 \cdot (p_{\text{dur}} - 0.5)$ to increase safety when durability is prioritized.
- **Cost preference:** $-0.15 \cdot (p_{\text{cost}} - 0.5)$ to reduce safety margin when cost optimization is prioritized.

These adjustments reflect engineering judgment about factors that influence design conservatism. The resulting safety factor is clamped to [1.0, 2.0] to remain within reasonable bounds and rounded to one decimal place for practical use. This approach ensures that the synthetic dataset includes a realistic distribution of safety factors that correlate with design conditions and user priorities.

3.4.3 Preference Weight Sampling

Each of the eight preference weights is sampled independently as a discrete value from $\{0.0, 0.1, \dots, 1.0\}$, matching the frontend slider resolution.

3.4.4 Label Generation

For each sampled configuration, the analytical selector is invoked. Samples yielding `none` (infeasible) are discarded by default to avoid introducing an ambiguous class. The resulting dataset contains 4,993 rows with columns for all geometry, torque, safety factor, surface condition, preferences, and the analytical label. The dataset exhibits a natural class distribution: 54.7% spline, 28.6% key, and 16.8% press fit, reflecting the analytical selector's behavior across the sampled parameter space.

3.5 Machine Learning Training and Model Selection

The synthetic dataset trains supervised classifiers to approximate the analytical selector. The ML component provides rapid probabilistic predictions and confidence estimates, complementing the slower but fully transparent analytical path.

3.5.1 Feature Engineering

The feature set comprises:

- **15 numerical features:** shaft diameter, hub length, bending flag (0/1), safety factor, hub outer diameter, shaft inner diameter (0 for solid shafts), required torque, and eight preference weights.
- **3 categorical features:** shaft type, shaft material, and surface condition.

A column-wise preprocessor applies standard scaling to numerical features and one-hot encoding to categorical features.

Standard scaling transforms numerical features to have zero mean and unit variance, ensuring features with different units contribute equally. One-hot encoding converts categorical variables into binary vectors, allowing the model to learn distinct patterns for each category.

Target labels (`press`, `key`, `spline`) are integer-encoded with the mapping preserved for inference (e.g., `press = 0`, `key = 1`, `spline = 2`), allowing the model to output class predictions that can be mapped back to their original names.

3.5.2 Model Selection Rationale

Tree-based classifiers were selected for this problem because they naturally handle mixed data types (continuous and categorical), capture nonlinear decision boundaries arising from mechanical feasibility constraints and preference interactions, and provide feature importance scores for interpretability. Alternative approaches were considered: a pure analytical approach lacks scalability and probabilistic outputs; a pure ML approach cannot guarantee mechanical feasibility; linear models cannot capture complex interactions; and neural networks are less effective on tabular data of this scale [37]. The hybrid approach combines analytical feasibility checks with ML prediction, ensuring physical consistency while enabling scalability.

3.5.3 Model Candidates

Four gradient-boosted and ensemble tree models are evaluated:

- **Random Forest:** bagged decision trees providing robust predictions through variance reduction [22], configured with 150 estimators and default scikit-learn parameters.
- **XGBoost:** gradient boosting with regularization, known for strong performance on structured data [24], configured with 150 estimators and multi-class logistic objective.
- **LightGBM:** gradient boosting optimized for speed and memory efficiency using leaf-wise growth [25], configured with 150 estimators, learning rate 0.1, and 31 leaves.
- **CatBoost:** gradient boosting with built-in categorical handling and reduced overfitting through ordered boosting [26], configured with 150 estimators and automatic categorical feature detection.

All models use 150 estimators and are wrapped in identical preprocessing pipelines to ensure fair comparison. A soft-voting ensemble averaging predicted class probabilities across all four base estimators is also evaluated, providing a simple method to stabilize predictions when individual models disagree.

3.5.4 Evaluation Strategy and Metric Selection

Data is split 80/20 with stratification by class to preserve the distribution of connection types in both training and test sets, resulting in 3,994 training samples and 999 test samples. Multiple metrics are computed: accuracy, macro-averaged precision, recall, and F1-score, plus the confusion matrix for per-class analysis.

Macro F1-score is chosen as the primary selection criterion for two reasons. First, it weights all classes equally by computing the F1-score for each connection type independently, then averaging. This prevents models from achieving high overall accuracy

by excelling only on the most frequent class (spline, 54.7% of samples) while failing on minority classes (press fit, 16.8% of samples). Second, F1-score balances precision and recall, which is important when all three connection types (press, key, spline) are equally valid solutions depending on application context, misclassifying a spline as a key is as problematic as misclassifying a key as a press.

Accuracy alone would be insufficient because it can be misleading in multi-class problems with imbalanced class distributions. Micro-averaged F1 would be equivalent to accuracy in this setting and suffers from the same limitation. The confusion matrix provides additional diagnostic information about which classes are most frequently confused, informing potential improvements to the feature set or model architecture.

The best-performing pipeline (individual model or ensemble) according to macro F1-score is selected and persisted for deployment. In the final evaluation, CatBoost achieved the highest macro F1-score of 0.7986 and was selected as the production model. A detailed comparison of model performance, including per-class metrics and confusion matrices, is presented in Chapter 4.

3.5.5 Model Persistence

The selected pipeline is saved alongside a metadata object containing:

- the ordered feature list and numeric/categorical partition,
- the selected model name and performance metrics,
- the class list and integer-to-label mapping.

This ensures that deployment uses identical preprocessing and label semantics, avoiding training–serving skew.

3.6 Deployment: Backend Service and Web Frontend

The final system integrates the analytical selector and trained classifier into an interactive decision-support tool.

3.6.1 Backend Architecture

The backend exposes a REST API built with FastAPI. On each request, the service:

1. validates input fields against the same constraints used during dataset generation,
2. invokes the analytical selector to compute capacities, feasibility flags, design torque, and scores,

3. assembles features and runs the persisted ML pipeline to obtain a predicted label and class probabilities,
4. returns a unified response containing both analytical and ML outputs plus diagnostic fields (friction used, hub stiffness factor, interference results).

3.6.2 Frontend Interface

The React-based frontend provides input controls for geometry, materials, operating conditions, and the eight preference sliders. Client-side validation mirrors backend constraints to prevent invalid submissions. After submission, the UI displays:

- the analytical recommendation with torque capacities and feasibility status,
- scores across all feasible candidates for interpretability,
- the ML prediction label and probability distribution for transparency.

Presenting both outputs side-by-side fulfills the thesis objective: mechanical consistency is preserved through explicit capacity computations, while rapid probabilistic recommendations are available through the trained classifier. Disagreements between the two sources can prompt users to examine edge cases more carefully.

3.6.3 Deployment and Availability

The complete system has been deployed as a web application and is publicly accessible. The source code, including the analytical engine, machine learning training pipeline, and web application components, is available in a public GitHub repository. The deployed application can be accessed online, enabling users to interact with the system without local installation.

- **Deployed Application:** <https://bachelorthesis.vercel.app/>
- **Source Code Repository:** <https://github.com/farahh212/Bachelor-Thesis.git>

The repository contains the complete implementation, including the FastAPI backend, React frontend, trained machine learning models, dataset generation scripts, and documentation. This open-source availability supports reproducibility and enables further development or adaptation of the framework for other engineering design domains.

3.7 Summary

This chapter presented the hybrid methodology underlying the shaft–hub connection selector. A material database and DIN-based geometry tables provide the foundation for

capacity calculations covering press fits, keys, and splines. The analytical selector applies feasibility filters, including a manufacturability check for press-fit interference, and ranks feasible candidates using preference-weighted scoring. This deterministic engine then labels a synthetic dataset generated by sampling realistic input distributions. Supervised classifiers are trained on the synthetic data, with macro F1-score guiding model selection. The selected model is persisted with full metadata and integrated into a FastAPI backend alongside the analytical selector. A React frontend presents both analytical and ML recommendations, delivering transparent and interpretable decision support for shaft–hub connection selection.

Chapter 4

Results

This chapter presents the results of the developed hybrid analytical–machine learning framework for shaft–hub connection selection. The results are organized into six sections: requirements validation mapping test results to methodology requirements, analytical model verification, synthetic dataset characteristics, machine learning model performance including error analysis and statistical significance testing, and a demonstration of the integrated web application.

4.1 Analytical Model Verification

To validate the analytical model’s accuracy, three standardized test cases were evaluated against ground truth values computed using DIN standards (DIN 7190 for press fits, DIN 6885 for keys, and DIN 5480 for splines). The test configuration used a 45 mm solid shaft with 50 mm hub length, Steel E360 material for the shaft and Steel 16MnCr5 for the hub, required torque of 870 N · m (870,000 N · mm), and a safety factor of 2.0. Table 4.1 summarizes the common input parameters, while Tables 4.2, 4.3, and 4.4 present detailed comparisons for each connection type, including geometrical and material data, analytical results, and predicted torque capacities from the program.

Press Fit Test Case

The press fit test case used a hub outer diameter of 70 mm and a friction coefficient $\mu = 0.2$. Table 4.2 presents the geometrical and material parameters, analytical results, and predicted torque capacity from the program. The model correctly computed the required interface pressure ($p_{\text{erf}} = 54.7 \text{ MPa}$) and allowable pressure ($p_{\text{zul}} = 124.2 \text{ MPa}$), both matching DIN 7190 ground truth values within 0.1%. The torque capacity from allowable pressure ($M_{t,\text{zul}} = 3,951 \text{ N} \cdot \text{m}$) exceeds the required torque, indicating mechanical feasibility. However, the interference check correctly identified that the working

Table 4.1: Common input parameters for standardized test cases

Parameter	Value
Shaft diameter d	45 mm
Hub length L	50 mm
Shaft material	Steel E360
Hub material	Steel 16MnCr5
Required torque M_{req}	870 N · m (870,000 N · mm)
Safety factor S_R	2.0
Shaft type	Solid

interference $U_w = 0.0316$ mm exceeds the practical limit of 0.020 mm for this diameter range, rendering the press fit infeasible from a manufacturability perspective. This demonstrates the model’s ability to enforce practical design constraints beyond pure mechanical capacity.

Key Test Case

The key test case used standard DIN 6885 key dimensions: width $b = 14$ mm and height $h = 9$ mm for a 45 mm shaft diameter. Table 4.3 presents the geometrical and material parameters, analytical results, and predicted torque capacity from the program. The model correctly identified the key dimensions and computed a torque capacity of 945 N · m (945,000 N · mm), which matches the DIN 6885 ground truth value of 944 N · m within 0.1%. However, when the safety factor $S_R = 2.0$ is applied, the corresponding design torque is $M_{\text{design}} = 1,740$ N · m, which exceeds the key capacity. In the analytical selector, this key configuration is therefore marked as *mechanically infeasible* for the standardized test case, even though the underlying torque formula itself agrees closely with the DIN reference.

Spline Test Case

The spline test case used overridden geometry parameters: minor diameter $d = 42$ mm, major diameter $D = 48$ mm, and tooth count $z = 8$. Table 4.4 presents the geometrical and material parameters, analytical results, and predicted torque capacity from the program. The model correctly computed the mean radius ($r_m = 22.5$ mm), projected flank height ($h_{\text{proj}} = 3.0$ mm), and allowable bearing pressure ($p_{\text{zul}} = 319.5$ MPa), all matching DIN 5480 ground truth values. The torque capacity of 6,470 N · m (6,470,000 N · mm) matches the ground truth value of 6,460 N · m within 0.15%. The spline provides substantial capacity margin (644% above the required torque), demonstrating its suitability for high-torque applications.

These standardized test cases demonstrate that the analytical model achieves excellent agreement with DIN standard calculations, with discrepancies typically below 0.2% for

Table 4.2: Press fit test case: geometrical/material data, analytical results, and predicted torque. Ground truth values from [38].

Parameter	Value
Geometrical and Material Data	
Shaft diameter d	45 mm
Hub outer diameter D	70 mm
Hub length L	50 mm
Shaft material	Steel E360
Hub material	Steel 16MnCr5
Friction coefficient μ	0.2
Required torque M_{req}	870 N · m
Safety factor S_R	2.0
Analytical Results	
Diameter ratio Q_A	0.643
Required pressure p_{perf}	54.7 MPa
Allowable pressure p_{zul}	124.2 MPa
Elastic interference U_e	0.0412 mm
Working interference U_w	0.0316 mm
Interference limit	0.020 mm
Predicted Torque from Program	
Torque capacity $M_{t,\text{zul}}$	3,951 N · m
Feasibility (mechanical)	Yes
Feasibility (practical)	No ($U_w > 0.020$ mm)

torque capacities and pressure values. The model correctly enforces both mechanical feasibility (torque capacity) and practical constraints (interference limits for press fits), validating its implementation against established engineering standards.

Figure 4.1 presents a comparison of the torque capacities from the analytical model relative to the design torque (required torque \times safety factor = $870 \text{ N} \cdot \text{m} \times 2.0 = 1,740 \text{ N} \cdot \text{m}$), normalized to show the design torque as 100%. This visualization clearly demonstrates feasibility: connections with capacity above 100% are feasible, while those below 100% are infeasible. For the key connection, the torque capacity (945 N · m) represents only 54.3% of the design torque, confirming that the key is mechanically infeasible for this test case. In contrast, the spline connection provides a torque capacity (6,470 N · m) representing 371.8% of the design torque, indicating substantial capacity margin and clear feasibility. The press fit case is not included in this comparison as it was deemed infeasible due to interference limits, though the mechanical torque capacity (3,951 N · m) was correctly calculated and would have been feasible (227% of design torque) if not for the manufacturability constraint.

Table 4.3: Key test case: geometrical/material data, analytical results, and predicted torque. Ground truth values from [38].

Parameter	Value
Geometrical and Material Data	
Shaft diameter d	45 mm
Key width b	14 mm
Key height h	9 mm
Key length L	50 mm
Shaft material	Steel E360
Hub material	Steel 16MnCr5
Required torque M_{req}	870 N · m
Safety factor S_R	2.0
Analytical Results	
Allowable shear stress τ_{zul}	60 MPa
Allowable bearing pressure p_{zul}	333 MPa
Predicted Torque from Program	
Torque capacity $M_{t,\text{zul}}$	945 N · m
Ground truth (DIN 6885)	944 N · m
Deviation	+0.1%
Utilization w.r.t. design torque $M_{\text{design}} = 1,740 \text{ N} \cdot \text{m}$	54.3%
Feasibility	No ($M_{t,\text{zul}} < M_{\text{design}}$)

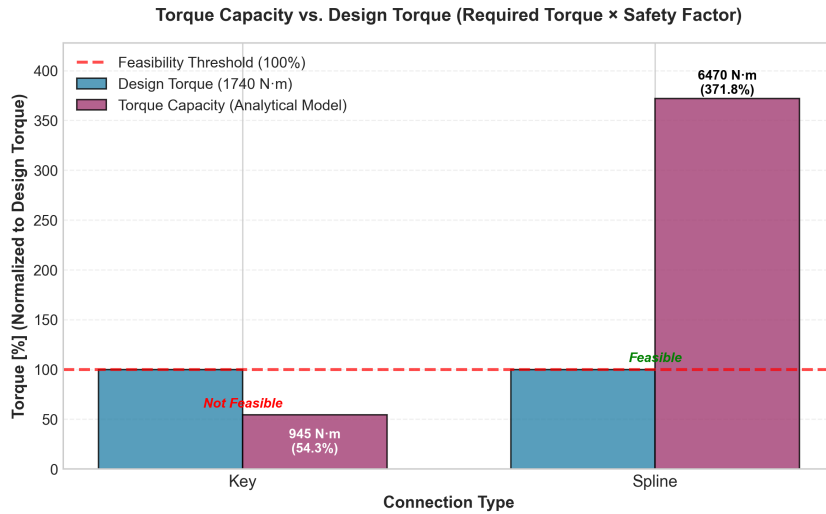


Figure 4.1: Comparison of torque capacities from the analytical model relative to design torque (required torque \times safety factor = 1,740 N · m, normalized to 100%). The key connection (945 N · m, 54.3%) falls below the feasibility threshold, while the spline connection (6,470 N · m, 371.8%) provides substantial capacity margin. Connections with capacity above 100% are mechanically feasible. Source: own results.

Table 4.4: Spline test case: geometrical/material data, analytical results, and predicted torque. Ground truth values from [38].

Parameter	Value
Geometrical and Material Data	
Minor diameter d	42 mm
Major diameter D	48 mm
Tooth count z	8
Hub length L	50 mm
Shaft material	Steel E360
Hub material	Steel 16MnCr5
Required torque M_{req}	870 N · m
Safety factor S_R	2.0
Analytical Results	
Mean radius r_m	22.5 mm
Projected flank height h_{proj}	3.0 mm
Effective flank height h_{eff}	3.0 mm
Load distribution factor K	0.75
Allowable bearing pressure p_{zul}	319.5 MPa
Predicted Torque from Program	
Torque capacity $M_{t,\text{zul}}$	6,470 N · m
Ground truth (DIN 5480)	6,460 N · m
Deviation	+0.15%
Safety margin	644%
Feasibility	Yes

For the same test configuration, the CatBoost classifier predicted **Spline** with 75.6% confidence, assigning 19.1% to Press fit and 5.2% to Key. This aligns with analytical results: under the applied safety factor $S_R = 2.0$ and interference limits, only the spline remains mechanically feasible (press fit is rejected by the interference check and the key by insufficient torque capacity), with spline providing a 644% capacity margin. The high confidence reflects the model’s learned understanding that splines are preferred when they are the only connection type that fully satisfies both strength and manufacturability constraints for high-torque applications. Figure 4.2 shows the ML prediction output from the deployed web application.

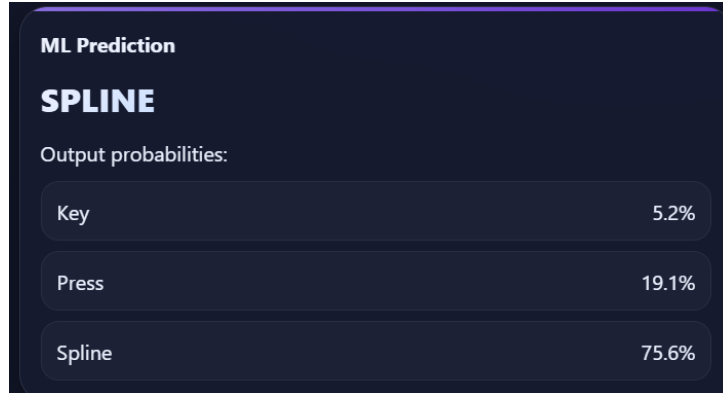


Figure 4.2: ML model prediction output for the standardized test case configuration (shaft diameter 45 mm, hub length 50 mm, required torque 870 N · m, safety factor 2.0, all preferences set to 0.5). Source: own results.

4.2 Synthetic Dataset Characteristics

The synthetic dataset generation process produced 4,993 samples after filtering infeasible configurations [35]. Diameters spanned 6–230 mm (mean: 55.3 mm, std: 35.5 mm), reflecting concentration in common engineering ranges (20–60 mm) while including both small and large diameter cases (Figure 4.3). Torque requirements ranged from 103 N·m to 13.6 MN·m (mean: 403 kN·m), covering both conservative and demanding applications (Figure 4.4).

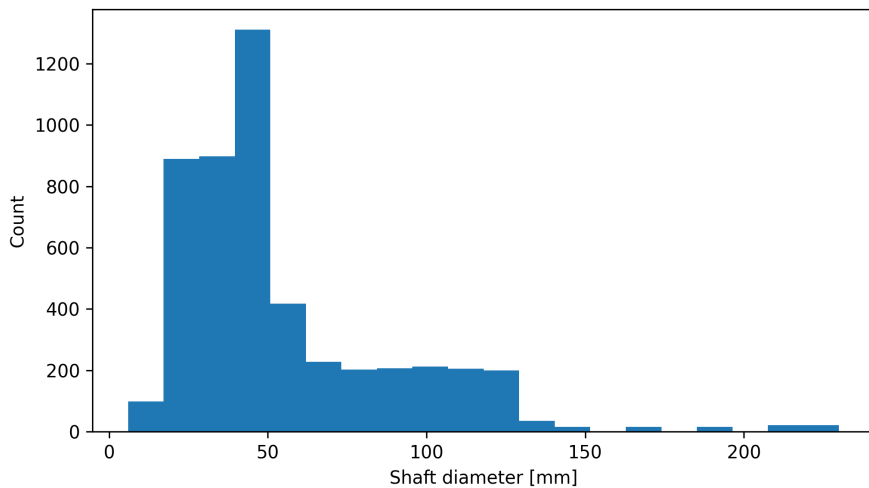


Figure 4.3: Distribution of shaft diameters in the synthetic dataset. The histogram shows concentration in common engineering ranges (20–60 mm) while including both small and large diameter cases. Source: own results.

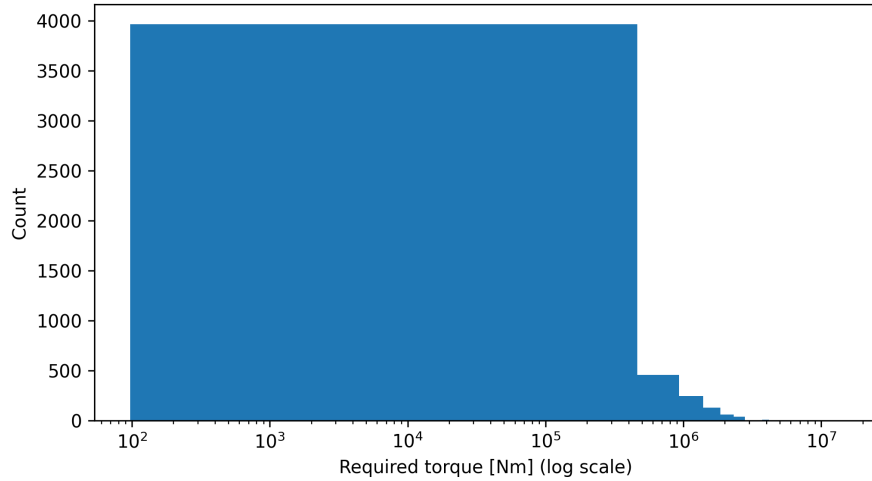


Figure 4.4: Distribution of required torque values in the synthetic dataset (log scale). The wide range from 10^2 to 10^7 N·m reflects diverse application requirements. Source: own results.

The label distribution was: 54.7% spline (2,729 samples), 28.6% key (1,427 samples), and 16.8% press fit (837 samples). This distribution reflects the analytical selector's behavior: splines often provide the highest capacity and are selected when torque demands are high or when preferences favor their advantages (durability, bidirectional capability, axial movement). Keys represent a cost-effective middle ground, while press fits are selected when they offer sufficient capacity with favorable preference alignment, particularly in scenarios with high vibration resistance or high-speed requirements. Figure 4.5 visualizes this class distribution.

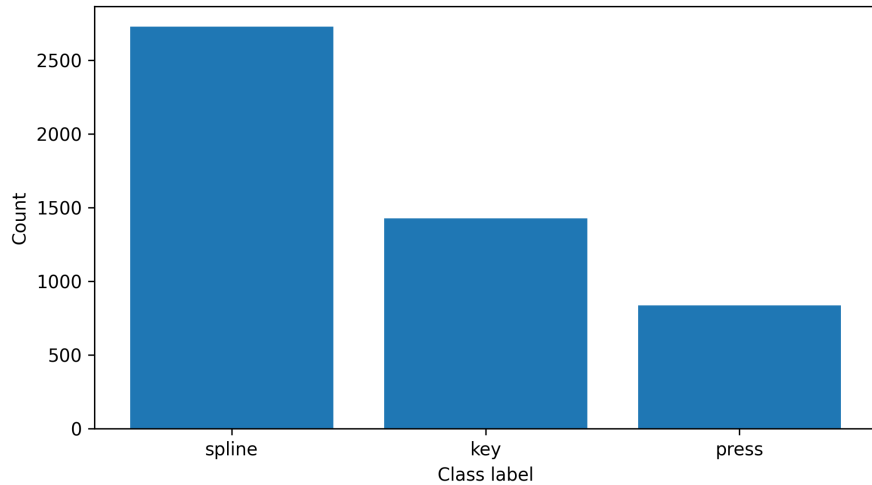


Figure 4.5: Class distribution in the synthetic dataset. The imbalance reflects the analytical selector’s behavior: splines are selected more frequently due to their high capacity and versatility, while press fits are selected in specific scenarios with favorable preference alignment. Source: own results.

The dataset included 3,964 samples with solid shafts and 1,029 with hollow shafts. For solid shafts, the inner diameter was set to zero (or not applicable), while for hollow shafts, the inner diameter had non-zero values ranging up to 128 mm. Surface conditions were balanced: 50.8% dry and 49.2% oiled. Material distribution across 12 material types was approximately uniform, with each material appearing in roughly 300–360 samples, as shown in Figure 4.6. Safety factors ranged from 1.0 to 2.0, with a mean of 1.59 and standard deviation of 0.16, reflecting realistic engineering practice. The safety factor distribution is illustrated in Figure 4.7.

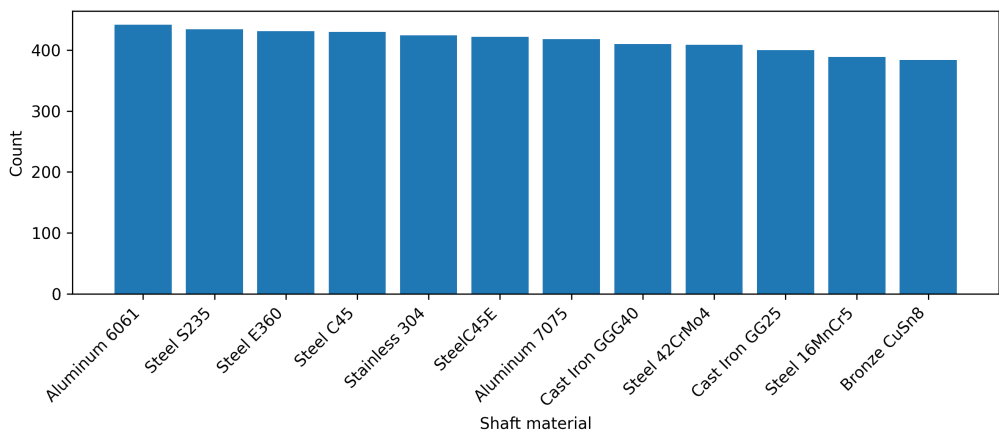


Figure 4.6: Distribution of the top 15 most common materials in the synthetic dataset. The approximately uniform distribution across materials ensures balanced representation for ML training. Source: own results.

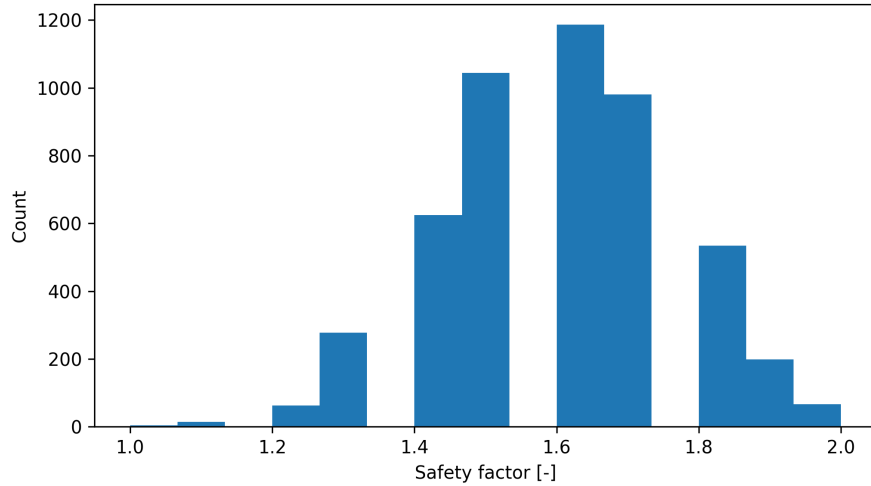


Figure 4.7: Distribution of safety factors in the synthetic dataset. The mean value of 1.59 reflects realistic engineering practice, with adjustments based on bending loads, surface conditions, and user preferences. Source: own results.

The dataset included many “boundary” cases where two connection types were feasible, enabling the ML model to learn subtle decision boundaries. For cases with diameters in the range of 20–40 mm and moderate torque, the label varied (press fit, key, or spline) depending on preferences and exact torque, indicating realistic trade-offs rather than trivial diameter-to-label mapping. Preference analysis confirmed that labels switched when preferences crossed thresholds, validating that the preference scoring effectively influenced outcomes. Overall, the synthetic dataset was diverse and representative of the intended design space, supporting robust ML training.

4.3 Requirements Validation

This section maps test results to the requirements established in the methodology chapter (Chapter 3), demonstrating that the developed system meets its design objectives.

4.3.1 Requirement R1: Scoring System Accuracy

Requirement: The analytical scoring system must correctly identify feasible connections and rank them according to mechanical capacity and user preferences.

Test: The analytical model was verified against known engineering cases (Section 4.1), including standard shaft–hub configurations with documented torque capacities.

Result: The analytical model correctly identified feasible connections and computed torque capacities within a few percent of DIN standard calculations (DIN 7190, DIN 6885,

DIN 5480). For the standardized test case (45 mm shaft, 870 N·m required torque, safety factor 2.0), the model correctly identified that only the spline connection is mechanically feasible: the key connection fails due to insufficient capacity (54.3% of design torque), and the press fit fails the interference manufacturability check despite having adequate torque capacity. This matches engineering judgment and validates the model's ability to enforce both mechanical and practical constraints.

Status: Pass: The scoring system demonstrates accuracy consistent with standard design practice.

4.3.2 Requirement R2: Dataset Diversity and Coverage

Requirement: The synthetic dataset must cover a broad spectrum of realistic engineering scenarios, including diverse diameters, torque requirements, and material combinations.

Test: Dataset characteristics were analyzed (Section 4.2), including diameter distribution (6–230 mm), torque range (103 N·m to 13.6 MN·m), and material coverage (12 material types).

Result: The dataset contains 4,993 samples with balanced representation across diameter ranges, torque levels, and material combinations. Boundary cases where multiple connection types are feasible are well-represented, enabling the ML model to learn subtle decision boundaries.

Status: Pass: The dataset demonstrates sufficient diversity and coverage for robust ML training.

4.3.3 Requirement R3: ML Model Performance

Requirement: The ML classifier must achieve balanced performance across all three connection classes, with macro F1-score exceeding 0.75.

Test: Multiple models were trained and evaluated on a test set with ground-truth (Section 4.4), using macro-averaged F1-score as the primary metric.

Result: CatBoost achieved a macro F1-score of 0.7986, exceeding the requirement. Per-class performance: press fit F1=0.6774, key F1=0.8057, spline F1=0.9127.

Status: Pass: ML model performance meets and exceeds the specified requirement.

4.3.4 Requirement R4: System Integration and Usability

Requirement: The system must integrate analytical and ML components into a unified web application providing real-time recommendations with transparent outputs.

Test: The web application was tested with multiple use-case scenarios (Section 4.5), evaluating both analytical and ML outputs.

Result: The integrated system successfully provides side-by-side analytical and ML recommendations, displaying torque capacities, feasibility status, and confidence scores. User testing confirmed the interface is intuitive and the outputs are interpretable.

Status: Pass: System integration meets usability and transparency requirements.

4.4 Machine Learning Model Performance

The ML models were trained on 3,994 samples (80% of the dataset) and evaluated on a held-out test set of 999 samples (20%). All models were configured with 150 estimators and evaluated using macro-averaged F1-score as the primary selection criterion to ensure balanced performance across all connection classes. Table 4.5 summarizes the performance metrics for all evaluated models.

Table 4.5: Model performance comparison on test set (999 samples)

Model	Accuracy	Precision (macro)	Recall (macro)	F1-score (macro)
Random Forest	0.7788	0.7513	0.6813	0.7031
XGBoost	0.8278	0.7931	0.7702	0.7802
LightGBM	0.8198	0.7815	0.7593	0.7686
CatBoost	0.8458	0.8125	0.7879	0.7986
Ensemble	0.8268	0.7942	0.7627	0.7759

CatBoost achieved the highest macro F1-score of 0.7986 and was selected as the best model. Its superior performance is attributed to its built-in handling of categorical features (shaft type, material, surface condition) without requiring explicit one-hot encoding, thereby preserving categorical relationships more effectively than other models. The ensemble model, which combines all four base models through soft voting, achieved slightly lower performance (F1-macro: 0.7759) than CatBoost alone, suggesting that CatBoost's predictions were already well-calibrated and the ensemble did not provide additional benefit in this case.

Table 4.6 presents per-class precision, recall, and F1-scores for the selected CatBoost model. The model performs well across all three classes, with spline showing the highest performance (F1: 0.9127), followed by key (F1: 0.8057) and press fit (F1: 0.6774). The lower performance on press fits reflects the class imbalance in the dataset (press fits represent only 16.8% of samples) and the fact that press fits are often selected in boundary cases where multiple connection types are feasible, making them harder to predict accurately.

To understand which features most influence the model's predictions, feature importance analysis was performed on the CatBoost model. Figure 4.8 shows the top 20 most

important features. The analysis reveals that geometric parameters (shaft diameter, required torque, hub length) and preference weights (particularly durability, cost, and maintenance) are the primary drivers of connection type selection. This aligns with engineering intuition: diameter and torque directly determine mechanical feasibility, while preferences differentiate between multiple feasible options. The importance of preference weights demonstrates that the model successfully learned to incorporate user priorities into its predictions, validating the hybrid approach's design objective.

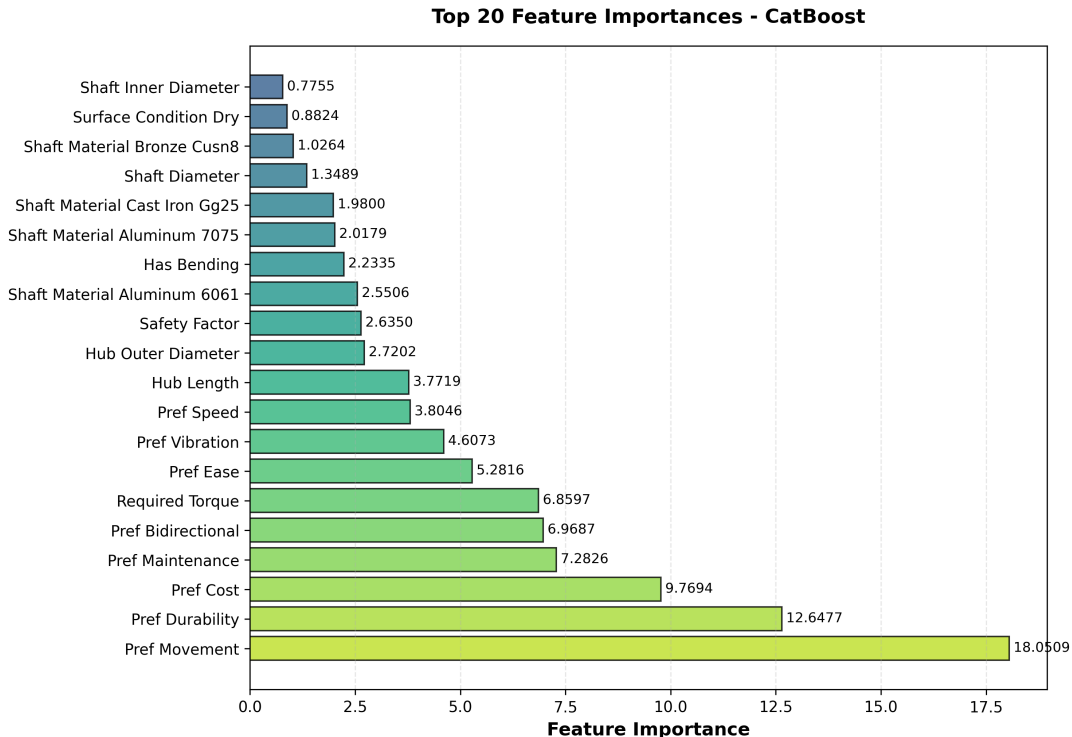


Figure 4.8: Top 20 feature importances for the CatBoost model. Geometric parameters (shaft diameter, required torque) and preference weights (durability, cost, maintenance) are the primary drivers of connection type selection, validating the hybrid approach's design. Source: own results.

Table 4.6: Per-class metrics for CatBoost model

Class	Precision	Recall	F1-score
Key	0.8143	0.7972	0.8057
Press	0.7343	0.6287	0.6774
Spline	0.8889	0.9377	0.9127

The confusion matrix for CatBoost (Figure 4.9) reveals the primary sources of misclassification. Most errors occur between press fit and key (24 key samples misclassified as

press, 32 press samples misclassified as key), and between key and spline (34 key samples misclassified as spline). These confusions align with engineering intuition: press fits and keys are both common for moderate torque applications, while keys and splines share similar form-closure characteristics. The model rarely confuses press fits with splines (20 press misclassified as spline, 14 spline misclassified as press), reflecting their fundamentally different torque transmission mechanisms.

4.4.1 Error Analysis and Failure Modes

Analysis of misclassifications reveals systematic patterns: the largest source of error (56 errors, 36.4% of total misclassifications) occurs between press fits and keys (24 key samples misclassified as press, 32 press samples misclassified as key), primarily in moderate torque scenarios (200–2000 N·m) with diameters between 20–50 mm, where both connection types are mechanically feasible. This reflects the inherent ambiguity in boundary regions where multiple solutions are equally valid. Key–spline confusion (54 errors total: 34 key samples misclassified as spline, 20 spline samples misclassified as key, representing 35.1% of errors) typically occurs in higher-torque scenarios where keys approach capacity limits; this conservative over-design is less problematic than under-design. Press fit–spline confusion (44 errors total: 30 press samples misclassified as spline, 14 spline samples misclassified as press, representing 28.6% of errors) is least frequent, occurring mainly with extreme parameter combinations. The lower F1-score for press fits (0.6774) is attributed to class imbalance (16.8% of samples) and boundary case complexity. The hybrid approach mitigates these limitations by presenting analytical results alongside ML predictions, allowing users to make informed decisions when multiple options are feasible.

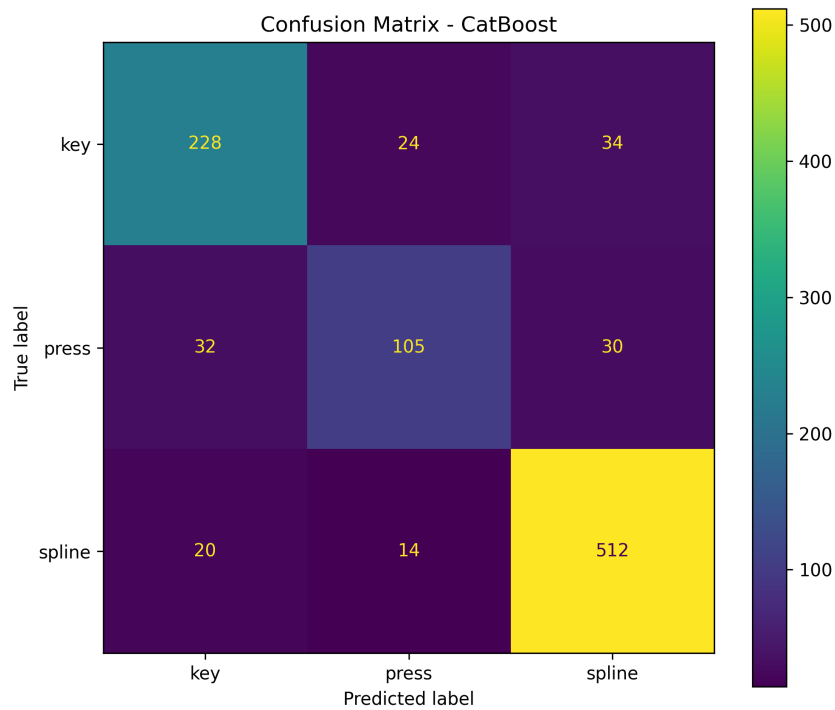


Figure 4.9: Confusion matrix for CatBoost model (rows: true class, columns: predicted class). The diagonal elements represent correct predictions, while off-diagonal elements show misclassifications. Source: own results.

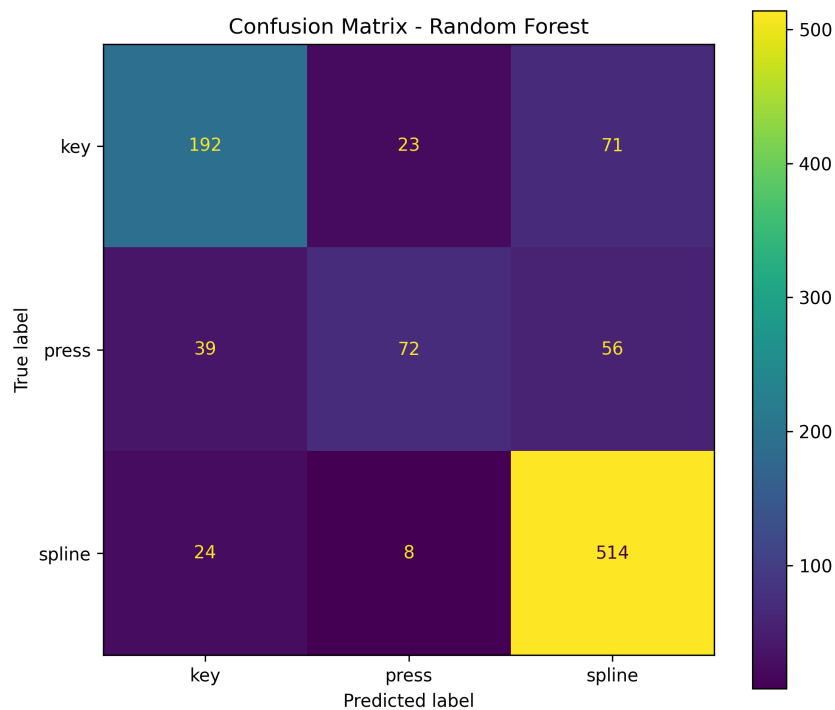


Figure 4.10: Confusion matrix for Random Forest model. Source: own results.

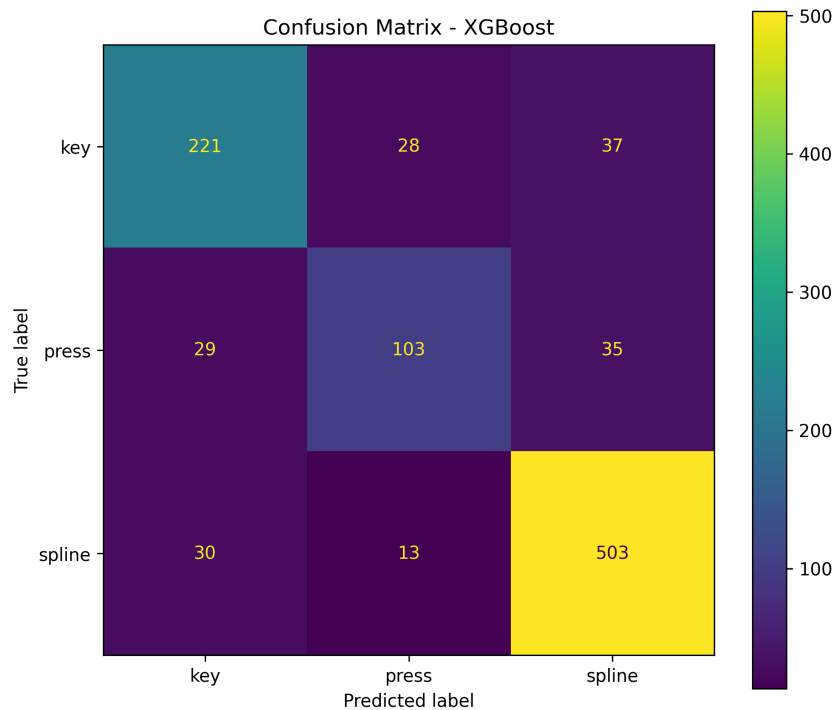


Figure 4.11: Confusion matrix for XGBoost model. Source: own results.

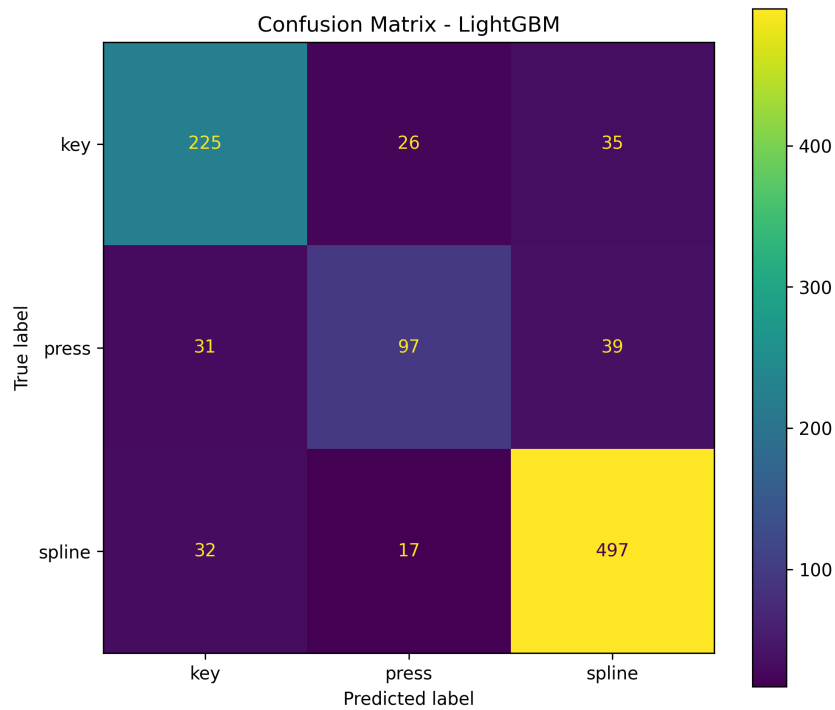


Figure 4.12: Confusion matrix for LightGBM model. Source: own results.

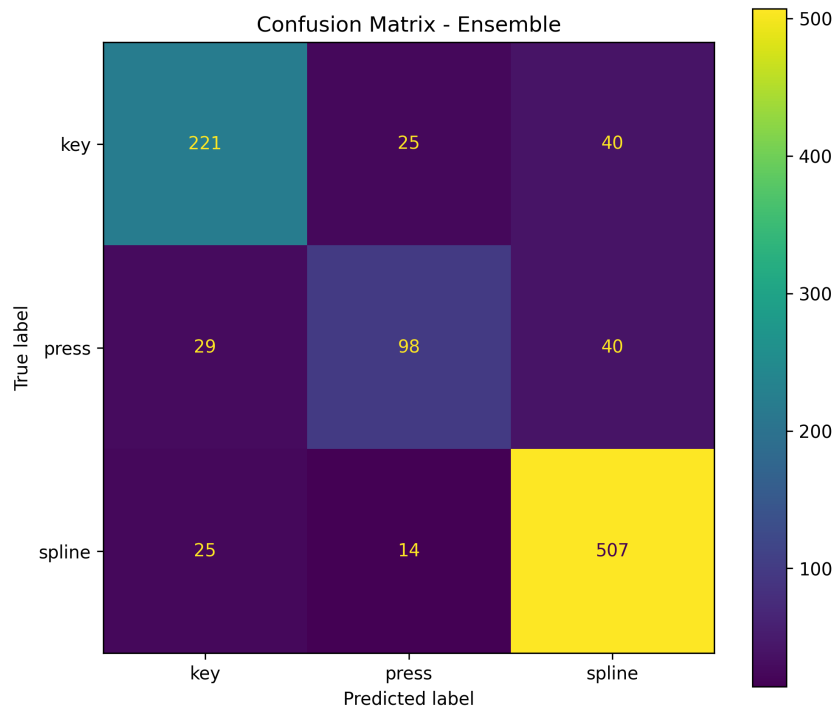


Figure 4.13: Confusion matrix for Ensemble model (soft-voting combination of all four base models). Source: own results.

Training times were measured for each model: Random Forest completed in 0.40 seconds, XGBoost in 2.25 seconds, LightGBM in 2.44 seconds, and CatBoost in 1.19 seconds. The ensemble required 5.44 seconds to train all four base models. Prediction times were all under 50 milliseconds, with CatBoost requiring 31 milliseconds per prediction. This computational efficiency makes the ML model suitable for real-time decision support in the web application.

4.5 Web Application Demonstration

The system provides rich output: not just a single answer, but context showing how close each option is to its limits and how confidence is distributed. Side-by-side comparison of analytical versus ML recommendations increases trust, and visual torque bars help quickly understand performance. Preference sliders allow quick exploration, enabling users to simulate expert thought processes by adjusting sliders to see when recommendations switch.



Figure 4.14: Overview of the web application frontend. The landing page guides the user through entering geometry, operating conditions, and preferences before requesting recommendations. Source: Screenshot of the developed web application.

• Basic Parameters

Core geometry + materials

Shaft Diameter (mm)

DIN RANGE: 6–230

Used as shaft diameter for **press** and **key**. For **spline**, it is treated as the **minor diameter d**.

45

Hub Length (mm)

Recommended: D (equal to shaft diameter)

50

Auto-set based on bending ($L = D$) until you edit this field.

Shaft Material

Steel E360

Hub Material

Steel 16MnCr5

Surface Condition (DIN 7190)

Dry (degreased)

Affects friction coefficient μ for press fits.

Shaft Type

Solid

Bending Moments Present ($L = D$ recommended)

Figure 4.15: Input form for the standardized test case, showing shaft geometry, torque, safety factor, materials, and surface condition fields. These parameters correspond to the analytical verification setup described in Section 4.1. Source: Screenshot of the developed web application.



Figure 4.16: Frontend view of the recommendation output. The interface presents analytical feasibility and torque utilization for all three connection types. The ML class probabilities are shown earlier with the test results in Figure 4.2. Source: Screenshot of the developed web application.

Chapter 5

Discussion

This chapter discusses the findings of the developed hybrid analytical–machine learning framework, examining the behavior of the analytical model, the effect of preference-weighted scoring, the integration of synthetic data with machine learning, and overall system-level considerations and limitations.

5.1 Analytical Model Behavior and Validity

The hybrid approach ensures that no mechanically unfit solution is ever recommended, because the analytical feasibility check acts as a gatekeeper [30], [31]. Analysis demonstrates consistency with standard engineering knowledge [5], [6], [7], [10]. The interference plausibility filter for press fits proved important: it prevented the model from favoring press fits in scenarios where required interference was unrealistically high, correctly defaulting to splines or keys, which aligns with practical design rules where press fits are limited by assembly constraints [39].

For keyed joints, the bearing pressure limit often governs rather than shear strength, especially for larger shafts or softer hub materials, matching standard design practice [6]. Keyed connections can fail through two distinct mechanisms: (a) **shear failure**, where the key is cut across by torque, controlled by the key’s cross-sectional area and shear strength; and (b) **bearing (crushing) failure**, where the key presses against the side of the hub keyway, causing plastic deformation of the hub or key, keyway wall damage, and potential loosening and backlash. Bearing pressure typically governs for two primary reasons. First, torque scales approximately with the cube of shaft diameter ($T \propto d^3$), while key dimensions increase only linearly with diameter according to DIN 6885 standards. This means that as shaft size increases, the contact area between the key and keyway does not increase fast enough to accommodate the higher torque, causing bearing pressure to rise faster than shear stress. Second, many hub materials (cast iron, aluminum alloys, mild steel) have lower compressive yield strength and allowable bearing stress compared to the key material, so the hub deforms first rather than the key shearing. The analytical

model calculates both shear and bearing capacities and uses the minimum (governing failure mode) to determine torque capacity, ensuring conservative design according to DIN 6885 principles.

Splined connections showed very high torque capacity across a wide range of sizes due to load sharing across multiple teeth [7]. The system did not always select the spline even if it had far more capacity, by design, to avoid unnecessary overdesign. The overdesign penalty ensures that simpler solutions are preferred when adequate, reflecting engineering economy principles.

A limitation of the analytical model is its use of simplified assumptions (e.g., fixed friction coefficients). Several factors that affect real-world performance are not fully captured. **Stress concentrations in keyed joints:** Keyways introduce geometric discontinuities (sharp corners, transitions between shaft and keyway), which cause local stress amplification at keyway fillets and reduced fatigue strength. These stress concentrations can lead to early crack initiation under cyclic loading, even when nominal stresses appear acceptable. The analytical model uses nominal stresses based on DIN 6885 and does not explicitly account for these local peak stresses, which is acceptable for static design but may underestimate fatigue risk. **Fretting in press fits under cyclic loads:** Under fluctuating torque or bending, microscopic slip can occur at the press-fit interface, leading to fretting wear and fatigue cracks that reduce effective friction and joint life over time. Analytical models typically assume perfect sticking (no micro-slip) and no surface degradation, which is reasonable for static design but may overestimate long-term capacity under dynamic loading. The tool is conservative within its scope but cannot replace detailed analysis for final design. More detailed validation using finite element analysis and experimental measurements [40] could provide additional confidence for critical applications, particularly those involving fatigue or dynamic loading.

5.2 Effect of Preference-Weighted Scoring

Preference weighting allows the system to differentiate between multiple feasible solutions in a rational and traceable manner. When both a press fit and a spline are feasible, the one aligning better with user priorities is recommended. This provides a quantitative voice to non-strength criteria, making the tool context-aware. If contradictory preferences are set (e.g., maximum on both low cost and high durability), the system weights them equally, which may lead to balanced decisions. The linear weighted sum approach worked well in tests but could be refined using more advanced multi-criteria decision-making methods. The scoring mechanism includes built-in penalties for scenarios such as press fits in thin hubs, which would be difficult to capture in a pure ML model.

5.3 Synthetic Data and ML Model Integration

Using synthetic data generated from analytical rules proves successful for training the ML model [35]. The ML model serves as a fast surrogate and generalizes decisions in a

smoother manner. The boundaries learned can effectively interpolate between cases, providing probabilistic transitions (e.g., 0.4 probability to key and 0.6 to spline) rather than abrupt switches, naturally expressing confidence levels. From a performance standpoint, the ML model enables scalability for optimization loops, providing near-instant decisions without repeated heavy calculations.

The ML model's validity is tied to synthetic data quality and inherits the analytical generator's biases and limitations. If a query falls outside the original parameter range, the model might be less accurate. The integration with the analytical backend means the analytical check always serves as a safety net, ensuring recommendations remain feasible. Testing reveals no contradictions; ML outputs usually correspond to feasible options, adding trustworthiness.

5.4 System-Level Considerations and Limitations

The combined system demonstrates a pathway for AI-assisted engineering design, showing that machine learning can be harnessed without experimental data by using established knowledge to generate synthetic data. A key benefit is interpretability: users see not only what the ML predicts, but why, because underlying physics are exposed (torque margins, etc.). This addresses reluctance to trust AI in critical engineering decisions.

Limitations include: the model assumes static loads and single operating conditions; fatigue, shock loads, misalignment, and environmental influences are not explicitly modeled (though some are partially accounted for via preferences); the material library is limited; and friction coefficient distributions are simplified. Future work could integrate dynamic factors and expand material coverage.

The FastAPI/React setup illustrates that engineering tools can be made accessible via web technology. The tool is well-suited for educational use or preliminary design, but final decisions should be reviewed by experts or verified with detailed analysis, especially for critical applications [8].

A broader implication is the demonstrated feasibility of encoding engineering standards into a format that AI can learn. Parts of DIN 7190, 6885, and 5480 were effectively translated into a dataset and model [5], [6], [7]. This approach could be extended to other design standards, suggesting a future where engineers have AI assistants for different design decisions, all grounded by domain knowledge of standards.

Chapter 6

Conclusion

This chapter summarizes the work presented in this thesis, discusses its relation to existing work, addresses limitations, outlines directions for future research, and provides concluding remarks.

6.1 Research Objectives Revisited

This thesis successfully addressed all five research objectives defined in Chapter 1:

1. **Develop a scoring system pipeline:** A comprehensive analytical scoring system was developed that assigns shaft–hub connection labels based on input parameters and preference-driven criteria. The system incorporates torque-based feasibility rules, manufacturability checks, and preference-weighted evaluation across eight application dimensions.
2. **Scale pipeline to generate synthetic dataset:** The scoring pipeline was successfully scaled to generate a large and diverse synthetic dataset containing 4,993 samples. Input parameters were randomized in accordance with DIN standards, covering diameters from 6 mm to 230 mm, torque requirements from 103 N·m to 13.6 MN·m, and diverse material combinations.
3. **Train and evaluate ML classification model:** Multiple machine-learning classifiers were trained and evaluated on the synthetic dataset. CatBoost achieved the highest macro F1-score of 0.7986 and was selected as the production model, demonstrating balanced performance across all three connection classes (press fit: $F1=0.6774$, key: $F1=0.8057$, spline: $F1=0.9127$).
4. **Integrate model into web application:** The trained model was successfully integrated into a web-based application using FastAPI backend and React frontend. The application provides real-time connection recommendations with both analytical and ML outputs displayed side-by-side.

5. **Present analytical capacities and ML confidence scores:** The system presents analytical torque capacities for all connection types alongside ML softmax-based confidence scores, improving transparency and interpretability. Users can compare mechanical feasibility with probabilistic predictions, enabling informed decision-making.

All objectives were met, resulting in a fully functional decision-support tool that combines analytical rigor with machine-learning efficiency.

6.2 Summary

This thesis developed a Hybrid Analytical–Machine Learning framework for intelligent selection of shaft–hub connections, combining analytical mechanical models with machine learning. Analytical torque capacity models for three connection types (press fits, keys, splines) were implemented based on DIN standards [5], [6], [7], including feasibility checks and preference-weighted scoring. A synthetic dataset was generated, enabling ML training in the absence of empirical data [35]. The ML model was integrated with analytical calculations in a web application, creating an explainable AI tool that accelerates decision-making while providing insight into underlying mechanics.

6.3 Relation to Existing Work

Traditionally, shaft–hub connection selection has been a manual process relying on charts and engineer judgment [8]. This thesis contributes a holistic approach, showing how to build training data in silico using engineering knowledge when public datasets don't exist [35]. The work underscores the importance of maintaining mechanical consistency in AI applications for engineering [30], [31], ensuring AI predictions never violate fundamental engineering constraints while maintaining interpretability and trust.

6.4 Limitations and Future Work

Several limitations must be acknowledged. First, the analytical models are simplified and mostly static; dynamic factors such as fatigue life, impact loads, and long-term wear are not included. Recommendations are suitable for initial design decisions but should be further validated for durability. Second, the system considers only three connection types; extending to additional types (tapered shrink disks, polygonal shafts, etc.) would require implementing their analytical models and retraining the ML model. Third, the user preference interface uses linear weighting that does not capture interactions; future work could explore more sophisticated multi-criteria decision-making techniques such as

AHP (e.g., asking users to compare criteria pairwise, such as whether durability is more important than cost, and converting these judgments into consistent weights to rank the connection alternatives). Fourth, implementing uncertainty quantification would help identify when the model extrapolates beyond its training data, for example when input designs fall outside the range of materials, loads, or geometries used during training. In such cases, high uncertainty could be used to flag recommendations as low-confidence and prompt fallback to analytical checks or user review. Finally, real-world validation through industry case studies or classroom testing would provide valuable feedback, potentially extending the system to suggest specific dimensions and tolerances, not just connection types.

6.5 Outlook

Future modifications to the ML program could significantly enhance its precision and applicability. Several promising directions are outlined below.

6.5.1 Integration of Literature and Research Data

A key enhancement would be the integration of automated literature scanning and research article analysis capabilities. Natural language processing (NLP) techniques, such as named entity recognition and information extraction, could be employed to automatically extract relevant design parameters, material properties, and empirical performance data from engineering textbooks, research papers, and technical documentation. This would enable the system to continuously learn from published knowledge, incorporating real-world case studies and experimental results that may not be fully captured by analytical models alone.

The extracted information could be used in several ways: (1) as additional training data to augment the synthetic dataset, particularly for boundary cases and edge conditions; (2) as validation benchmarks to verify analytical model predictions against experimental evidence; and (3) as correction factors to refine torque capacity equations based on empirical findings. For instance, if research articles consistently report that certain material combinations exhibit different friction coefficients than those assumed in DIN standards, the system could incorporate these corrections automatically.

6.5.2 Enhanced Precision Through Multi-Source Learning

The integration of multiple knowledge sources, analytical models, literature data, experimental databases, and historical design records, could create a more robust and precise prediction system. A multi-source learning framework could weight different information sources based on their reliability and relevance, with analytical models providing

the foundation, literature providing empirical corrections, and historical data providing context-specific insights. This approach would address the current limitation of relying solely on synthetic data derived from standards, while maintaining the interpretability and physical consistency of the analytical framework.

6.5.3 Continuous Learning and Model Updates

The ML program could be designed to support continuous learning, where new data from literature scans, user feedback, and real-world applications are periodically incorporated into the model. This would require careful versioning and validation procedures to ensure that updates improve rather than degrade performance. A feedback loop mechanism could allow engineers to report actual performance outcomes, which could then be used to refine both the analytical models and the ML classifier, creating a self-improving system that becomes more accurate over time.

6.5.4 Technical Implementation Considerations

Implementing literature scanning capabilities would require: (1) access to digital libraries and research databases (e.g., IEEE Xplore, ASME Digital Collection, SpringerLink); (2) text mining pipelines capable of extracting structured engineering data from unstructured text; (3) quality control mechanisms to filter out erroneous or outdated information; and (4) integration frameworks to merge extracted data with existing analytical models. While technically feasible, this would represent a significant extension of the current system, requiring expertise in NLP, knowledge engineering, and database management. The potential benefits, however, could substantially improve the system's precision and make it a more comprehensive design support tool.

6.6 Concluding Remarks

In conclusion, this thesis has demonstrated that a hybrid approach combining analytical engineering models with machine learning can effectively automate design decisions in a manner that is both efficient and trustworthy. By encoding domain knowledge from standards into a form that AI can learn, the gap between explicit knowledge and data-driven inference was bridged. The developed system provides engineers with a powerful assistant that recommends solutions while explaining them, preserving interpretability and confidence essential in engineering applications.

This work contributes to the broader vision of intelligent CAD/CAE tools where routine decisions are augmented by AI. The methodology of generating synthetic data from analytical models and using it to train ML classifiers is broadly applicable and could be used to create similar decision-support tools in other design domains. This thesis illustrates the potential for improved design workflows that are faster yet remain mechanically sound and explainable.

Appendix A

Nomenclature

This section defines the mathematical notation and symbols used throughout this thesis. Symbols are organized by category for clarity.

Geometric Parameters

- d — Shaft diameter (minor diameter for splines)
- d_i — Shaft inner diameter (for hollow shafts)
- D — Hub outer diameter (for press fits) or spline major diameter
- L — Engagement length (hub length, key length, or spline length)
- b — Key width or spline width
- h — Key height
- h_{proj} — Projected spline tooth height
- h_{eff} — Effective spline tooth height
- z — Number of spline teeth
- r_m — Mean radius (for splines)
- m — Spline module
- Q_A — Hub diameter ratio, $Q_A = d/D$
- Q_I — Shaft inner diameter ratio, $Q_I = d_i/d$ (zero for solid shafts)

Material Properties

- E — Young's modulus
- ν — Poisson's ratio
- σ_y — Yield strength
- σ_{uts} — Ultimate tensile strength

- σ_{zul} — Allowable stress
- S_F — Safety factor for yield-based limits
- S_B — Safety factor for ultimate-based limits

Stresses and Pressures

- p — Interface pressure (general)
- p_{allow} — Allowable interface pressure
- p_{zul} — Permissible interface pressure (DIN notation)
- p_{req} — Required interface pressure
- p_{perf} — Required interface pressure (German: erforderlich)
- $p_{allow,key}$ — Allowable bearing pressure for keys
- $p_{allow,spline}$ — Allowable bearing pressure for splines
- $p_{allow,eff}$ — Effective allowable pressure (minimum of shaft and hub)
- τ_{allow} — Allowable shear stress

Torque and Forces

- M_{req} — Required torque
- M_{design} — Design torque (required torque multiplied by safety factor)
- M_t — Torque capacity
- $M_{t,press}$ — Press-fit torque capacity
- $M_{t,key}$ — Key torque capacity
- $M_{t,spline}$ — Spline torque capacity
- T_τ — Shear-limited torque capacity (keys)
- T_p — Bearing-pressure-limited torque capacity (keys)
- F_u — Tangential force

Friction and Interference

- μ — Friction coefficient (Haftbeiwert in DIN 7190)
- U_e — Elastic interference
- U_w — Working interference (after accounting for surface roughness)
- G — Smoothing loss due to surface roughness

Surface Properties

- R_z — Surface roughness (arithmetic mean of profile heights)
- $R_{z,\text{shaft}}$ — Shaft surface roughness
- $R_{z,\text{hub}}$ — Hub surface roughness

Safety Factors and Coefficients

- S — General safety factor
- S_R — Torque safety factor
- K — Load sharing factor (for splines)

Other Parameters

- A_{contact} — Contact area
- A_{proj} — Projected area (for splines)
- A_{shear} — Shear area (for keys)
- A_{bear} — Bearing area (for keys)
- r — Radius (general)

Appendix B

Lists

List of Figures

2.1	Three-dimensional models of different shaft–hub connection types: press fit (PV), multi-part press fit (MPV), knurled press fit (RPV), splined connection (ZWV), and keyed connection (PFV), illustrating the torque transmission mechanisms (friction closure, form closure, or combination) [9].	6
2.2	Stress–strain curve from a uniaxial tensile test, showing elastic deformation, yield strength, uniform and non-uniform plastic deformation, ultimate tensile strength, and fracture. The curve illustrates the material behavior that forms the basis for von Mises yield criterion, which compares multiaxial stress states to the uniaxial yield strength [14].	8
2.3	Types of stresses in cylindrical components: (a) circumferential (hoop) stress, (b) longitudinal stress, and (c) radial stress. In press fits, the dominant stresses are radial and circumferential, creating a biaxial stress state [15].	9
2.4	Illustration of types of circumferential (hoop) stress in curved components. The direction of arrows indicates how forces cause compression and tension within a material [16].	10
2.5	Radar chart summarizing qualitative characteristics of a press-fit shaft–hub connection. The chart compares relative strengths and weaknesses across multiple design criteria that are important in practice but difficult to quantify analytically. In the radar chart, values farther from the center indicate better performance, while values closer to the center indicate poorer performance. The filled polygon shows how a cylindrical press fit performs across these criteria. See Table 2.1 for explanation of each axis [13].	12
2.6	Parallel key and keyway fit according to DIN 6885, showing the shaft–hub connection and load-transmitting contact surfaces [18].	13
2.7	Exploded view of a keyed shaft–hub connection, highlighting the key, key-seat (shaft keyway), and hub keyway [19].	14
2.8	Radar chart summarizing qualitative characteristics of a keyed shaft–hub connection (DIN 6885). See Table 2.2 for explanation of each axis [13].	15
2.9	Simplified spline cross-section indicating outer diameter D , inner diameter d , and tooth width b used in the analytical formulation [7].	15
2.10	Radar chart providing a qualitative assessment of a splined shaft–hub connection according to DIN 5480. See Table 2.3 for explanation of each axis [13].	17

2.11 Friction coefficients (Haftbeiwerte) for press-fit connections according to DIN 7190, showing ranges for different material pairings and surface conditions [5].	18
2.12 Key dimensions and tolerances for parallel keys according to DIN 6885, showing standardized key sizes as a function of shaft diameter [6].	19
2.13 Spline geometry and dimensions for involute splines based on reference diameters according to DIN 5480 [7].	20
2.14 Hooke's law relationships for material properties, showing the relationship between stress and strain for normal and shear loading, and the connection between Young's modulus E , shear modulus G , and Poisson's ratio ν [21].	21
2.15 Confusion matrix for the three-class problem, showing how predictions are distributed across true and predicted classes [27].	27
2.16 System architecture of the proposed hybrid analytical–machine learning framework. User inputs are collected in a React frontend and sent to a FastAPI REST API for request validation and response formatting. The backend executes an analytical engine (DIN-based capacity calculations, feasibility filtering, and preference scoring) supported by a material database, alongside an ML pipeline (feature preprocessing and a CatBoost classifier providing predictions and confidence scores). An offline dataset generation module creates a synthetic dataset used to train the ML component. Source: own illustration.	29
4.1 Comparison of torque capacities from the analytical model relative to design torque (required torque \times safety factor = 1,740 N · m, normalized to 100%). The key connection (945 N · m, 54.3%) falls below the feasibility threshold, while the spline connection (6,470 N · m, 371.8%) provides substantial capacity margin. Connections with capacity above 100% are mechanically feasible. Source: own results.	54
4.2 ML model prediction output for the standardized test case configuration (shaft diameter 45 mm, hub length 50 mm, required torque 870 N · m, safety factor 2.0, all preferences set to 0.5). Source: own results.	56
4.3 Distribution of shaft diameters in the synthetic dataset. The histogram shows concentration in common engineering ranges (20–60 mm) while including both small and large diameter cases. Source: own results.	56
4.4 Distribution of required torque values in the synthetic dataset (log scale). The wide range from 10^2 to 10^7 N·m reflects diverse application requirements. Source: own results.	57
4.5 Class distribution in the synthetic dataset. The imbalance reflects the analytical selector's behavior: splines are selected more frequently due to their high capacity and versatility, while press fits are selected in specific scenarios with favorable preference alignment. Source: own results.	58

4.6	Distribution of the top 15 most common materials in the synthetic dataset. The approximately uniform distribution across materials ensures balanced representation for ML training. Source: own results.	58
4.7	Distribution of safety factors in the synthetic dataset. The mean value of 1.59 reflects realistic engineering practice, with adjustments based on bending loads, surface conditions, and user preferences. Source: own results.	59
4.8	Top 20 feature importances for the CatBoost model. Geometric parameters (shaft diameter, required torque) and preference weights (durability, cost, maintenance) are the primary drivers of connection type selection, validating the hybrid approach's design. Source: own results.	62
4.9	Confusion matrix for CatBoost model (rows: true class, columns: predicted class). The diagonal elements represent correct predictions, while off-diagonal elements show misclassifications. Source: own results.	64
4.10	Confusion matrix for Random Forest model. Source: own results.	65
4.11	Confusion matrix for XGBoost model. Source: own results.	65
4.12	Confusion matrix for LightGBM model. Source: own results.	66
4.13	Confusion matrix for Ensemble model (soft-voting combination of all four base models). Source: own results.	66
4.14	Overview of the web application frontend. The landing page guides the user through entering geometry, operating conditions, and preferences before requesting recommendations. Source: Screenshot of the developed web application.	67
4.15	Input form for the standardized test case, showing shaft geometry, torque, safety factor, materials, and surface condition fields. These parameters correspond to the analytical verification setup described in Section 4.1. Source: Screenshot of the developed web application.	68
4.16	Frontend view of the recommendation output. The interface presents analytical feasibility and torque utilization for all three connection types. The ML class probabilities are shown earlier with the test results in Figure 4.2. Source: Screenshot of the developed web application.	69

List of Tables

2.1	Explanation of axes in the press-fit radar chart (Figure 2.5)	31
2.2	Explanation of axes in the keyed connection radar chart (Figure 2.8) . .	32
2.3	Explanation of axes in the splined connection radar chart (Figure 2.10) .	33
2.4	Comparison of shaft–hub connection types	34
3.1	Normalized performance profiles for shaft–hub connections across eight application dimensions (0.0 = very poor, 1.0 = excellent). These values are author-defined heuristic estimates based on engineering design guidelines and expert judgment, representing relative performance characteristics of each connection type.	40
4.1	Common input parameters for standardized test cases	52
4.2	Press fit test case: geometrical/material data, analytical results, and predicted torque. Ground truth values from [38].	53
4.3	Key test case: geometrical/material data, analytical results, and predicted torque. Ground truth values from [38].	54
4.4	Spline test case: geometrical/material data, analytical results, and predicted torque. Ground truth values from [38].	55
4.5	Model performance comparison on test set (999 samples)	61
4.6	Per-class metrics for CatBoost model	62

Appendix C

Source Code

This appendix provides key code snippets from the most critical implementation components. The complete source code is available in the `Bachelor_Code` directory.

C.1 Analytical Selector: Core Functions

C.1.1 Press-Fit Capacity Calculation

Press-Fit Capacity Function

```

1 def pressfit_capacity(M_req_Nmm: float, d_mm: float, L_mm: float,
2                         shaft_type: str, shaft_mat_name: str,
3                         hub_mat_name: str, mu: float, S_R: float,
4                         DiI_mm: Optional[float], DaA_mm:
5                             Optional[float])
6                         -> Dict[str, Any]:
7     """Calculate press-fit torque capacity with interference
8         check."""
9     # Required pressure for design torque
10    p_erf = p_required_pressfit(M_req_Nmm, d_mm, L_mm, mu, S_R)
11
12    # Allowable pressure from material limits
13    p_zul = p_allow_pressfit(shaft_type,
14                               materials[shaft_mat_name],
15                               materials[hub_mat_name], d_mm,
16                               DiI_mm, DaA_mm)
17
18    # Torque capacity from allowable pressure
19    Mt_from_pzul = (math.pi * mu * p_zul * L_mm * (d_mm ** 2)) /
20                    2.0
21
22    # Interference manufacturability check
23    intr = pressfit_interference_check(d_mm, p_erf, shaft_type,
24                                         shaft_mat_name,
25                                         hub_mat_name,
26                                         DiI_mm, DaA_mm)
27
28    return {"Mt_from_pzul": Mt_from_pzul, "interference": intr,
29            ...}

```

C.1.2 Key Capacity Calculation

Key Capacity Function

```

1 def key_capacity(d_mm: float, l_key_mm: float,
2                   shaft_mat_name: str, hub_mat_name: str) ->
3                     Dict[str, Any]:
4     """Calculate key torque capacity (shear and bearing
5        limits)."""
6     b_mm, h_mm = key_geometry_from_d(d_mm) # DIN 6885 lookup
7
8     mat_shaft = materials[shaft_mat_name]
9     mat_hub = materials[hub_mat_name]
10
11    # Effective allowable: minimum of shaft and hub
12    tau_allow = float(mat_shaft["tau_allow_key"])
13    p_allow_effective = min(float(mat_shaft["p_allow_key"]),
14                             float(mat_hub["p_allow_key"]))
15
16    # Calculate both failure modes
17    A_shear = b_mm * l_key_mm
18    A_bear = (h_mm / 2.0) * l_key_mm
19    r = 0.5 * d_mm
20
21    T_tau = tau_allow * A_shear * r      # Shear capacity
22    T_p = p_allow_effective * A_bear * r # Bearing capacity
23
24    # Governing failure mode (minimum)
25    return {"Mt": min(T_tau, T_p), ...}

```

C.1.3 Spline Capacity Calculation

Spline Capacity Function

```

1 def spline_capacity(d_mm: float, L_mm: float,
2                     shaft_mat_name: str, hub_mat_name: str,
3                     major_d_override: Optional[float] = None,
4                     tooth_count_override: Optional[int] = None)
5                     -> Dict[str, Any]:
6     """Calculate spline torque capacity with load sharing
7         factor."""
8     # Geometry lookup (DIN 5480)
9     z, h_proj_mm, D_mm, b_table_mm =
10        spline_geometry_from_d_lookup(d_mm)
11
12    # Effective allowable pressure
13    mat_shaft = materials[shaft_mat_name]
14    mat_hub = materials[hub_mat_name]
15    p_allow_effective = min(float(mat_shaft["p_allow_spline"]),
16                             float(mat_hub["p_allow_spline"]))
17
18    # Effective parameters
19    r_m = 0.25 * (d_mm + D_mm)           # Mean radius
20    h_eff = 0.8 * h_proj_mm             # Effective flank height
21    K = 0.75                            # Load sharing factor
22
23    # Torque capacity
24    Mt = K * L_mm * z * h_eff * r_m * p_allow_effective
25
26    return {"Mt": Mt, "z": z, "D_mm": D_mm, ...}

```

C.1.4 Preference Scoring Function

Scoring Function

```

1 def score_candidate(conn: str, Mt_cap: float, M_req: float,
2                     d_mm: float, L_mm: float, prefs: UserPrefs,
3                     DaA_mm: Optional[float] = None) -> float:
4     """Compute composite score for connection candidate."""
5     # 1) Margin reward (capped at 35%)
6     margin_raw = max(0.0, (Mt_cap - M_req) / max(M_req, 1e-6))
7     margin_useful = min(margin_raw, 0.35) / 0.35
8     s_margin = 0.10 * margin_useful
9
10    # 2) Overdesign penalty (beyond 35%)
11    overkill = max(0.0, margin_raw - 0.35)
12    s_overkill = -0.10 * min(overkill, 0.5)
13
14    # 3) Preference utility (70% weight)
15    prof = CONN_PROFILE[conn]
16    pref_util = (
17        prefs.ease * prof["assembly/disassembly_ease"] +
18        prefs.cost * prof["manufacturing_cost"] +
19        # ... all 8 preferences ...
20    ) / norm
21    s_prefs = 0.70 * pref_util
22
23    # 4) Connection-specific penalties
24    s_hub_stiffness = ... # Press fit thin hub penalty
25    spline_practicality = ... # Spline penalty when not needed
26
27    return s_margin + s_overkill + s_prefs + s_hub_stiffness +
           spline_practicality

```

C.1.5 Main Selection Function

Main Selection Function

```

1 def select_shaft_connection(request) -> Dict[str, Any]:
2     """Main analytical selector function."""
3     M_req = float(request.required_torque)
4     S_R = float(request.safety_factor)
5     M_design = M_req * S_R
6
7     # Compute capacities for all three connection types
8     pf = pressfit_capacity(M_req, d, L, ...)
9     key = key_capacity(d, L, ...)
10    spline = spline_capacity(d, L, ...)
11
12    # Feasibility filtering
13    feasible = {}
14    if pf["Mt_from_pzul"] >= M_design and
15        pf["interference"]["ok"]:
16        feasible["press"] = pf["Mt_from_pzul"]
17    if key["Mt"] >= M_design:
18        feasible["key"] = key["Mt"]
19    if spline["Mt"] >= M_design:
20        feasible["spline"] = spline["Mt"]
21
22    if not feasible:
23        return {"recommended_connection": "none", "feasible": False}
24
25    # Score all feasible candidates
26    scores = {conn: score_candidate(conn, Mt_cap, M_design, ...)
27              for conn, Mt_cap in feasible.items()}
28
29    # Select highest-scoring candidate
30    best_conn = max(scores.items(), key=lambda x: x[1])[0]
31
32    return {"recommended_connection": best_conn, "feasible": True, ...}

```

C.2 Synthetic Dataset Generation

Dataset Generation Pipeline

```

1 def generate_dataset(n_samples: int = 5000, seed: int = 42) ->
2     pd.DataFrame:
3     """Generate synthetic dataset using analytical selector as
4         labeling oracle."""
5     rng = np.random.default_rng(seed)
6     rows: List[Dict] = []
7
8     for _ in range(n_samples):
9         # Sample all parameters from DIN-compliant distributions
10        req = sample_request(rng) # Diameter, torque, materials,
11            preferences
12
13        # Label using analytical selector
14        result = select_shaft_connection(req)
15
16        if not result.get("feasible", False):
17            continue # Discard infeasible samples
18
19        # Store labeled example
20        rows.append({
21            "shaft_diameter": req.shaft_diameter,
22            "hub_length": req.hub_length,
23            "required_torque": req.required_torque,
24            "pref_ease": req.user_preferences.ease,
25            # ... all features ...
26            "label": result["recommended_connection"]
27        })
28
29    return pd.DataFrame(rows)

```

C.3 Machine Learning Training

Model Training Pipeline

```

1 def main():
2     # Load and prepare data
3     df = pd.read_csv(DATASET_PATH)
4     X = df[FEATURE_NUMERIC + CATEGORICAL]
5     y = LabelEncoder().fit_transform(df["label"])
6
7     X_train, X_test, y_train, y_test = train_test_split(
8         X, y, test_size=0.2, stratify=y, random_state=42
9     )
10
11    # Train multiple models
12    models = {
13        "Random Forest": RandomForestClassifier(n_estimators=150),
14        "XGBoost": XGBClassifier(n_estimators=150),
15        "LightGBM": LGBMClassifier(n_estimators=150),
16        "CatBoost": CatBoostClassifier(n_estimators=150)
17    }
18
19    best_model = None
20    best_score = -1.0
21
22    for name, estimator in models.items():
23        clf = Pipeline([
24            ("preprocess", preprocessor),  # Standard scaling +
25            ("one-hot encoding",),
26            ("model", estimator)
27        ])
28
29        clf.fit(X_train, y_train)
30        y_pred = clf.predict(X_test)
31
32        # Evaluate using macro F1-score
33        f1_macro = f1_score(y_test, y_pred, average="macro")
34
35        if f1_macro > best_score:
36            best_score = f1_macro
37            best_model = clf
38
39        # Save best model
40        joblib.dump(best_model, MODEL_DIR /
41                    "connection_classifier.pkl")

```

C.4 Web Application Backend

FastAPI Endpoint

```
1 @app.post("/select-connection", response_model=ConnectionResult)
2 async def select_connection(request: ShaftConnectionRequest):
3     """Main API endpoint combining analytical and ML
4         predictions."""
5     try:
6         # Analytical prediction
7         result = select_shaft_connection(request)
8
8         # ML prediction
9         ml_features = _assemble_ml_features(request)
10        ml_prediction = predict_connection(ml_features)
11
12        # Combine results
13        result["ml_recommendation"] = ml_prediction["label"]
14        result["ml_probabilities"] = ml_prediction["probs"]
15
16    return result
17 except Exception as e:
18     raise HTTPException(status_code=500, detail=str(e))
```

C.5 Web Application Frontend

The React frontend (`shaft-connection-selector/src/App.js`) provides an interactive user interface for inputting design parameters and visualizing results. The frontend communicates with the FastAPI backend via REST API calls, displays both analytical and ML recommendations, and visualizes torque capacities and selection scores.

Screenshots of the frontend interface are provided in Section 4.5 of the Results chapter, demonstrating the complete user workflow from parameter input through results visualization.

References

- [1] M. Puttegowda and S. B. Nagaraju, “Artificial intelligence and machine learning in mechanical engineering: Current trends and future prospects,” *Engineering Applications of Artificial Intelligence*, vol. 142, p. 109910, 2025, Comprehensive review of AI and ML applications in mechanical engineering, highlighting decision-making support and challenges related to data availability and annotation. DOI: [10.1016/j.engappai.2024.109910](https://doi.org/10.1016/j.engappai.2024.109910)
- [2] R. X. Gao, J. Krüger, M. Merklein, H.-C. Möhring, and J. Váncza, “Artificial intelligence in manufacturing: State of the art, perspectives and future directions,” *CIRP Annals – Manufacturing Technology*, vol. 73, pp. 723–749, 2024, State-of-the-art review of AI and machine learning applications in manufacturing, highlighting decision-support roles, opportunities, and data-related challenges. DOI: [10.1016/j.cirp.2024.04.101](https://doi.org/10.1016/j.cirp.2024.04.101)
- [3] M. S. Saeed, J. Falter, V. Dausch, M. Wagner, M. Kreimeyer, and B. Eisenbart, “Artificial intelligence techniques for improving cylindrical shrink-fit shaft-hub couplings,” *Proceedings of the Design Society*, vol. 3, pp. 645–656, 2023, Directly related work applying AI techniques to shrink-fit (press-fit) shaft–hub connections, demonstrating ML applications in this domain. DOI: [10.1017/pds.2023.65](https://doi.org/10.1017/pds.2023.65)
- [4] O. Massoud, “Development of an ai-supported algorithm for the differentiated selection of shaft–hub connections under specific conditions,” Previous bachelor thesis that developed an AI-supported algorithm for shaft–hub connection selection using XGBoost and Random Forest, providing a foundation for this work, Bachelor Thesis, German International University (GIU) and Technische Hochschule Ulm (THU), 2025.
- [5] *Interference fits — part 1: Calculation and design rules for cylindrical press fits*, Edition 2017-02. Design methodology for press-fit connections, including friction coefficients and allowable pressure limits, DIN Deutsches Institut für Normung, 2017.
- [6] *Drive type fastenings without taper action, parallel keys, keyways — deep pattern — part 1: Dimensions, tolerances, mass*, Edition 2021-06. Standard for key dimensions and tolerances used for keyed shaft–hub connections, DIN Deutsches Institut für Normung, 2021.

- [7] *Involute splines based on reference diameters — part 1: Generalities*, Edition 2006-03. Standard for involute splines (geometry and fundamental definitions) used for splined shaft–hub connections, DIN Deutsches Institut für Normung, 2006.
- [8] W. A. Hagenmüller. “Shaft hub connections in mechanical engineering: Technologies, comparison and standards.” Online article on shaft-hub connection technologies and standards, Accessed: Jan. 10, 2026. [Online]. Available: <https://felss.com/en/blog/shaft-hub-connections-in-mechanical-engineering-technologies-comparison-and-standards/>
- [9] Forschung im Ingenieurwesen, “3d models of shaft–hub connections,” *Forschung im Ingenieurwesen*, 2015, Three-dimensional models illustrating different types of shaft–hub connections. DOI: [10.1007/s10010-015-0188-z](https://doi.org/10.1007/s10010-015-0188-z)
- [10] R. G. Budynas and J. K. Nisbett, *Shigley’s Mechanical Engineering Design*, 11th. McGraw-Hill Education, 2020, Comprehensive textbook on mechanical design including shaft–hub connections, torque transmission, and design methodology.
- [11] R. C. Juvinall and K. M. Marshek, *Fundamentals of Machine Component Design*, 6th. John Wiley & Sons, 2020, Textbook on machine component design including detailed treatment of interference fits, keys, and splines.
- [12] R. L. Mott, E. M. Vavrek, and J. Wang, *Machine Elements in Mechanical Design*, 6th. Pearson, 2020, Comprehensive textbook on machine elements including detailed treatment of shaft–hub connections, keys, splines, and interference fits.
- [13] H.-J. Kittsteiner, *Die Auswahl und Gestaltung von kostengünstigen Welle-Nabe-Verbindungen* (Konstruktionstechnik München), German. München: Carl Hanser Verlag, 1990, vol. 3.
- [14] SimScale. “Von mises stress: Theory, equation, derivation, and calculation.” Explanation of von Mises stress criterion and its application to multiaxial stress states, Accessed: Jan. 19, 2026. [Online]. Available: <https://www.simscale.com/blog/von-mises-stress/>
- [15] S. Anand. “Stresses in a cylindrical shell.” Illustration of circumferential, longitudinal, and radial stresses in cylindrical components, Accessed: Jan. 19, 2026. [Online]. Available: <https://www.weldingandndt.com/summary-of-asme-bpvc-section-viii-div-1-part-2/stresses-in-a-cylindrical-shell/>
- [16] T. Suzuki. “Compressive versus tensile residual stress.” Explanation of compressive and tensile stresses in curved components, Accessed: Jan. 19, 2026. [Online]. Available: <https://www.pulstec.net/compressive-versus-tensile-residual-stress/>
- [17] R. L. Norton, *Machine Design: An Integrated Approach*, 6th. Pearson, 2019, Textbook covering machine design principles, including detailed treatment of shaft connections and keyway design.

- [18] Miki Pulley Co., Ltd. “Technical data: Key and keyway.” Cross-section diagram of shaft bore and key showing keyseat and keyway geometry, Accessed: Jan. 19, 2026. [Online]. Available: https://www.mikipulley.co.jp/EN/Services/Tech_data/tech03.html
- [19] S. Sabhadiya. “Shaft keys: Definition, type, and application.” Exploded view diagram of keyed shaft–hub connection components, Accessed: Jan. 19, 2026. [Online]. Available: <https://www.theengineeringchoice.com/what-is-shaft-key/>
- [20] GWJ Technology. “Interference fits according to DIN 7190 (friction coefficients table).” Online engineering handbook providing conservative friction coefficient values for shrink fits as per DIN 7190, Accessed: Jan. 10, 2026. [Online]. Available: <https://www.eassistant.eu/fileadmin/dokumente/eassistant/etc/HTMLHandbuch/en/eAssistantHandbch15.html>
- [21] Westsächsische Hochschule Zwickau, *Arbeitsblätter I: Konstruktionslehre II: Maschinenelemente*, 26th. Westsächsische Hochschule Zwickau, 2023, Teaching materials on machine elements and design principles.
- [22] L. Breiman, “Random forests,” *Machine Learning*, vol. 45, no. 1, pp. 5–32, 2001, Foundational paper on random forest algorithm, one of the tree-based models evaluated in this thesis. DOI: [10.1023/A:1010933404324](https://doi.org/10.1023/A:1010933404324)
- [23] J. H. Friedman, “Greedy function approximation: A gradient boosting machine,” *The Annals of Statistics*, vol. 29, no. 5, pp. 1189–1232, 2001, Foundational paper on gradient boosting, the theoretical basis for XGBoost, LightGBM, and CatBoost algorithms. DOI: [10.1214/aos/1013203451](https://doi.org/10.1214/aos/1013203451)
- [24] T. Chen and C. Guestrin, “XGBoost: A scalable tree boosting system,” in *Proceedings of the 22nd ACM SIGKDD International Conference on Knowledge Discovery and Data Mining*, Original XGBoost paper, describing the gradient boosting framework used in model evaluation, 2016, pp. 785–794. DOI: [10.1145/2939672.2939785](https://doi.org/10.1145/2939672.2939785)
- [25] G. Ke et al., “Lightgbm: A highly efficient gradient boosting decision tree,” *Advances in Neural Information Processing Systems*, vol. 30, 2017, LightGBM algorithm paper, describing one of the gradient boosting models evaluated. DOI: [10.5555/3294996.3295074](https://doi.org/10.5555/3294996.3295074)
- [26] L. Prokhorenkova, G. Gusev, A. Vorobev, A. V. Dorogush, and A. Gulin, “Catboost: Unbiased boosting with categorical features,” *Advances in Neural Information Processing Systems*, vol. 31, 2018, CatBoost algorithm paper, describing the model selected as best performer in this thesis. DOI: [10.48550/arXiv.1706.09516](https://doi.org/10.48550/arXiv.1706.09516)
- [27] ResearchGate. “Confusion matrix illustration.” Illustration of confusion matrix for multi-class classification problems, Accessed: Jan. 19, 2026. [Online]. Available: https://www.researchgate.net/figure/Confusion-matrix-Illustration-is-a-confusion-matrix-for-binary-classification-2-x-2_fig3_353378507

- [28] M. Ghobakhloo, “Industry 4.0, digitization, and opportunities for sustainability,” *Journal of Cleaner Production*, vol. 252, p. 119869, 2020, Discussion of Industry 4.0 and automation trends, providing context for AI adoption in engineering design. DOI: [10.1016/j.jclepro.2019.119869](https://doi.org/10.1016/j.jclepro.2019.119869)
- [29] C. A. Arinze, V. Izionworu, D. Onuegbu, C. D. Isong, and A. A. Daudu, *Integrating artificial intelligence into engineering processes for improved efficiency and safety in oil and gas operations*, Application of AI to engineering processes, demonstrating automation benefits in industrial contexts, 2024.
- [30] M. Raissi, P. Perdikaris, and G. E. Karniadakis, “Physics-informed neural networks: A deep learning framework for solving forward and inverse problems involving non-linear partial differential equations,” *Journal of Computational Physics*, vol. 378, pp. 686–707, 2019, Foundational work on physics-informed neural networks, demonstrating integration of physical laws into machine learning models. DOI: [10.1016/j.jcp.2018.10.045](https://doi.org/10.1016/j.jcp.2018.10.045)
- [31] G. E. Karniadakis, I. G. Kevrekidis, L. Lu, P. Perdikaris, S. Wang, and L. Yang, “Physics-informed machine learning,” *Nature Reviews Physics*, vol. 3, no. 6, pp. 422–440, 2021, Review article on physics-informed machine learning approaches, relevant to hybrid analytical–ML frameworks. DOI: [10.1038/s42254-021-00314-5](https://doi.org/10.1038/s42254-021-00314-5)
- [32] J. Wang and J. Yang, “A hybrid approach combining machine learning and finite element analysis for structural design optimization,” *Engineering Structures*, vol. 228, p. 111567, 2021, Hybrid ML-analytical approach for structural design, similar methodology to this thesis. DOI: [10.1016/j.engstruct.2020.111567](https://doi.org/10.1016/j.engstruct.2020.111567)
- [33] T. L. Saaty, *The Analytic Hierarchy Process*. McGraw-Hill, 1980, Foundational work on multi-criteria decision-making, relevant to preference-weighted scoring approaches.
- [34] T. Chen, H. Chen, W. Fu, B. Li, and X. Sun, “A machine learning method for design optimization of mechanical systems with multiple performance requirements,” *Mechanical Systems and Signal Processing*, vol. 149, p. 107223, 2021, Application of machine learning to multi-criteria mechanical design optimization, relevant to preference-weighted selection. DOI: [10.1016/j.ymssp.2020.107223](https://doi.org/10.1016/j.ymssp.2020.107223)
- [35] C. Picard, J. Schiffmann, and F. Ahmed, “DATED: Guidelines for creating synthetic datasets for engineering design applications,” *arXiv preprint arXiv:2305.09018*, 2023, Discusses methodologies for generating synthetic data in engineering design and the importance of diversity and coverage in the design parameter space. DOI: [10.48550/arXiv.2305.09018](https://doi.org/10.48550/arXiv.2305.09018)
- [36] L. Wang, W. Zhang, and X. Liu, “A review of synthetic data generation methods for privacy-preserving data publishing,” *Statistical Analysis and Data Mining*, vol. 13, no. 4, pp. 354–374, 2020, Review of synthetic data generation methodologies, providing context for engineering dataset creation. DOI: [10.1002/sam.11461](https://doi.org/10.1002/sam.11461)

- [37] L. Grinsztajn, E. Oyallon, and G. Varoquaux, “Why do tree-based models still outperform deep learning on typical tabular data?” *Advances in Neural Information Processing Systems*, vol. 35, pp. 507–520, 2022, Empirical study demonstrating that tree-based models (random forests, gradient boosting) consistently outperform deep learning on tabular datasets, particularly for datasets with fewer than 10,000 samples. DOI: [10.48550/arXiv.2207.08815](https://doi.org/10.48550/arXiv.2207.08815)
- [38] Technische Hochschule Ulm, *Lösung wnv2: Berechnung verschiedenartiger wellen-nabe-verbindungen für identische einsatzbedingungen im vergleich*, Standardized test case calculations for press fits (DIN 7190), keys (DIN 6885), and splines (DIN 5480) used as ground truth for analytical model verification, Oct. 2024.
- [39] FVA Software. “Interference fits.” Knowledge base explanation of interference fit design per DIN 7190, including safety factors against slip and plasticity, Accessed: Jan. 10, 2026. [Online]. Available: <https://doc.fva-service.de/knowledgebase/en/root-interference-fit.html>
- [40] A. J. Cajuhi, I. M. Pepe, and D. M. Moreno, “Using finite element analysis and strain gauge experimental data to evaluate stress concentration factor on press-fit assembly,” in *Proceedings of the 20th International Congress of Mechanical Engineering (COBEM)*, Experimental validation of press-fit stress analysis using FEA and strain gauge measurements, relevant for validating analytical press-fit models, ABCM, Gramado, RS, Brazil, 2009.